Charge exchange of $^{229(m)}$Th ions in carbon foils

Ines Amersdorffer

München 2018

Ladungsaustausch von $^{229(\mathrm{m})}$Th-Ionen in Kohlenstofffolien

Bachelorarbeit

von

Ines Amersdorffer

geboren in Dachau

Fakultät für Physik

LUDWIG-MAXIMILIANS-UNIVERSITÄT MÜNCHEN

München 2018

Erstgutachter: PD Dr. Peter G. Thirolf

Tag der Abgabe: 14.08.2018

Tag der mündlichen Prüfung: 17.08.2018

Abstract

The most precise time measurements at present are achieved with atomic clocks. However, it has been proposed that they could be outperformed by nuclear clocks, using a nuclear transition instead of an atomic shell transition.

^{229}Th possesses an isomeric first excited state, denoted by $^{229\mathrm{m}}$Th, exhibiting an extraordinary low energy of only about 7.8 eV, an energy range that is reachable by existing laser technology. For this reason, it is the only nucleus which currently comes into consideration for the development of a nuclear clock. However, for its realization, precise knowledge of the nuclear transition energy is required.

One of the decay channels of $^{229\mathrm{m}}$Th is internal conversion (IC). An upcoming experiment performed in our group aims to determine the isomeric energy by measuring the kinetic energy of the electrons set free during the internal conversion decay of $^{229\mathrm{m}}$Th. In the experimental approach, the ^{229}Th isomer is populated in the α decay of a ^{233}U source placed in a buffer-gas stopping cell and an isotopically pure $^{229(\mathrm{m})}$Th ion beam is formed. As internal conversion only occurs in neutral $^{229\mathrm{m}}$Th atoms, it is essential to neutralize the thorium ions prior to a precise energy determination.

In the measurements presented in this thesis, it is shown that an efficient neutralization of thorium ions is accomplished by sending $^{229(\mathrm{m})}$Th ions through a carbon foil in which charge exchange occurs. The resulting neutral atoms can be isolated from any other positively or negatively charged particles generated in the neutralization process. The results can be used to perform a nearly background-free measurement of the nuclear transition energy via the detection of the IC electrons emitted from free $^{229\mathrm{m}}$Th atoms.

In a further experiment, the charge state distribution of the ions exiting the carbon foil is examined with an electrostatic analyzer consisting of a curved plate capacitor. The performance of the analyzer is tested in simulations (using the ion optics simulator SIMION 8.1) and experiments. A clear separation of different exit charge states can be achieved, which allows to select one of them for further examination. Such a setup can be used to create a pure $^{229(\mathrm{m})}\mathrm{Th}^{1+}$ ion beam and thus to investigate the unexpectedly short isomeric lifetime in $^{229}\mathrm{Th}^{1+}$, whose precise determination is still pending.

Zusammenfassung

Die heutzutage genauesten Zeitmessungen werden mit Atomuhren erzielt. Jedoch wurde vorgeschlagen, dass diese von Kernuhren übertroffen werden könnten, welche statt eines Elektronenüberganges in der Atomhülle einen Kernübergang verwenden.
^{229}Th besitzt einen isomeren ersten angeregten Kernzustand, bezeichnet als $^{229\mathrm{m}}$Th, der eine außergewöhnlich geringe Anregungsenergie von nur ca. 7.8 eV aufweist, ein Energiebereich, welcher mit vorhandener Lasertechnologie erreicht werden kann. Deshalb ist es der einzige Kern, welcher derzeit für die Entwicklung einer Kernuhr in Betracht kommt. Für deren Verwirklichung bedarf es jedoch einer genaueren Kenntnis der Isomerenergie.
Einer der Zerfallskanäle von $^{229\mathrm{m}}$Th ist die "innere Konversion". Das Ziel eines bevorstehenden Experiments unserer Arbeitsgruppe ist es, die Isomerenergie zu bestimmen, indem die Energie der Elektronen, die während des inneren Konversionszerfalls entstehen, gemessen wird. In dem experimentellen Ansatz wird das ^{229}Th-Isomer aus dem α-Zerfall einer ^{233}U-Quelle, eingebaut in eine Puffergas-Stop-Zelle, generiert und ein isotopenreiner $^{229(\mathrm{m})}$Th-Ionenstrahl erzeugt. Da der innere Konversionszerfall nur in neutralen $^{229\mathrm{m}}$Th-Atomen auftritt, ist es notwendig, die Ionen vor einer präzisen Energiebestimmung zu neutralisieren.
Mithilfe der in dieser Arbeit dargelegten Messungen kann gezeigt werden, dass eine effiziente Neutralisation von $^{229(\mathrm{m})}$Th-Ionen durch Ladungsaustausch in einer Kohlenstofffolie erreicht werden kann. Die Neutralatome können von anderweitigen positiv oder negativ geladenen Teilchen, welche im Neutralisationsprozess entstanden sind, separiert werden. Die Ergebnisse können genutzt werden, um eine nahezu untergrundfreie Messung der Übergangsenergie über den Nachweis der Elektronen durchzuführen, welche beim inneren Konversionszerfall von freien $^{229\mathrm{m}}$Th-Atomen entstehen.
In einem weiteren Experiment wird die Verteilung der Ladungszustände der aus der Kohlenstofffolie hinausfliegenden Ionen mit einem elektrostatischen Analysator, bestehend aus einem gekrümmten Plattenkondensator, untersucht. Das Leistungsvermögen des Analysators wird mit Simulationen (unter Nutzung des ionenoptischen Simulationsprogrammes SIMION 8.1) und im Experiment getestet. Eine Trennung der verschiedenen Ladungszustände wird erreicht. Dies macht es möglich, einen von ihnen für weitere Untersuchungen auszuwählen. Ein solcher Aufbau kann genutzt werden, um einen reinen $^{229(\mathrm{m})}$Th^{1+}-Ionenstrahl zu erzeugen und damit die unerwartet kurze Lebensdauer des Isomers in ^{229}Th^{1+} zu untersuchen, dessen genaue Bestimmung bis heute aussteht.

Contents

1 Introduction and Motivation

The measurement of time has always played an important role in science as well as in society. Many different ways for time measurement have been developed over the past centuries, however, the fundamental principle of time measurement remained unchanged.
A clock essentially consists of two parts: a physical package (e.g. an oscillator) that changes with time in a well-defined way and a device, which detects those changes (e.g. counts the oscillations) and transfers them into a value of time. For example, in a pendulum clock, the harmonic oscillation of the pendulum is translated to periodically recurring pulses. Those pulses can then be counted by the mechanical part of the pendulum clock and displayed.
What started off with sundials, hourglasses and candle clocks, led mankind to more and more sophisticated timekeeping devices due to technological progress. The most precise time measurements at present are achieved with atomic clocks. In optical atomic clocks, the frequency of light, which corresponds to a certain transition of an electron between two atomic shell orbitals, is used as a reference frequency.
There are two concepts for the realization of a modern optical atomic clock. There is either a laser-cooled single ion retained in a Paul trap or about 10^4 neutral atoms confined in an optical lattice. In both cases a spectroscopy laser is locked to the ultra-stable frequency of an atomic shell transition using a feedback system. The frequency is counted with the help of a frequency comb and can thus be transferred into a time value.

Today's optical clocks already provide an exceptional accuracy of about 10^{-18} [1]. This corresponds to an error of 1s after $3 \cdot 10^{10}$ years, which is considerably longer than the age of the universe. However, for some applications it would be useful to measure time even more precisely. The accuracy of the best atomic clocks today is restricted by the influence of external perturbations, e.g. as generated by occurrent magnetic and electric fields.
The nucleus of an atom is known to be significantly smaller than the atomic shell, which results in considerably smaller magnetic and electric momenta with a consequential higher resilience to external influences.
Based on these considerations it has been proposed that atomic clocks could potentially be

outperformed by a nuclear clock [2], where the frequency standard is set by a nuclear transition instead of an atomic shell transition. This could lead to an enhancement of accuracy of about one order of magnitude compared to even the best optical atomic clock operational today (resulting in an accuracy in the range of 10^{-19} [3]).
A nuclear clock may therefore, like other ultraprecise optical clocks, give advantages for clock-based geodesy, to take more precise measurements of the earth's gravitational field [4] and could also be used as a detection device in the search for (topological) dark matter [5]. Furthermore, it could help us to investigate potential time variations of fundamental constants like the fine structure constant α [6].

At present, the only nuclear transition that comes into consideration for such a nuclear clock, making use of already existing technology, is the transition between the ground state and the first excited nuclear state in ^{229}Th. It has the lowest excitation energy of all known nuclear states, lying in the eV region instead of the usual keV to MeV region for nuclear transitions. Given that such a low energy can be reached by today's laser technology, this is the only nuclear state where optical laser excitation could possibly be achieved in the near future. However, to allow for optical laser excitation of this exceptionally low-lying nuclear state, the value of the transition energy has to be known more precisely.
The determination of the nuclear transition energy of the first excited nuclear state (called an isomeric state due to its long lifetime of about several 1000 seconds) in ^{229}Th (denoted by $^{229\mathrm{m}}$Th) has therefore been subject to experimental investigations for decades. The reported values for the transition energy have been varying a lot, as is shown in Fig. 1.1, and so far all knowledge originated from indirect energy measurements (except for the most recent value which, however, has not been published in a peer-reviewed journal). The currently most accepted value is (7.8 ± 0.5) eV, corresponding to (159 ± 10) nm [11]. This value is not sufficiently precise in order to allow for direct $^{229\mathrm{m}}$Th laser excitation, e.g. in a Paul trap. For this reason, nuclear laser excitation of $^{229\mathrm{m}}$Th has not yet been achieved.

It is the objective of the experiments performed in our group, to determine the isomeric excitation energy directly for the first time via the isomer-to-ground-state decay of ^{229}Th. This direct measurement has the potential to pin down the isomer's transition energy with sufficient precision to allow for direct nuclear laser excitation. In these experiments, the recently detected decay of the excited nuclear state via internal conversion (IC) [13] is used. The kinetic energy of the electron emitted in the IC process can be measured, e.g., by a magnetic bottle spectrometer. This energy can be used to derive the isomeric transition energy. The decay via internal conversion is energetically forbidden in thorium ions and only occurs in neutral thorium. For this reason, the neutralization of $^{229(\mathrm{m})}$Th ions poses a

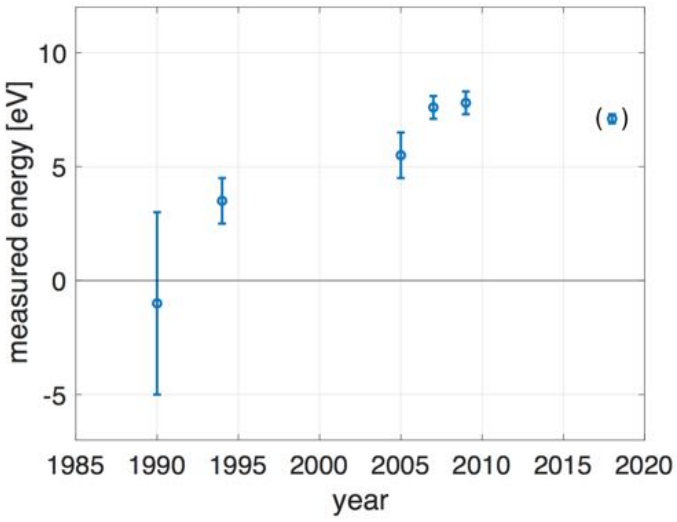

Figure 1.1: Historic evolution of the reported values (and their uncertainties) for the isomeric excitation energy of ^{229}Th. The values can be found in Refs. [7–12].

central aspect of the experimental setup.

In this thesis, the experimental aim is to test the neutralization of thorium ions in carbon foils. Not only neutral $^{229(\mathrm{m})}$Th atoms are generated in this process, but possibly also singly charged ions. The population of those is examined with regard to the still pending lifetime measurement of $^{229\mathrm{m}}\mathrm{Th}^{1+}$.

Therefore, two aspects are investigated in this thesis. The central objective is to prove the efficient neutralization of thorium ions in carbon foils like graphene. A secondary objective is the quantification of the population of $^{229(\mathrm{m})}\mathrm{Th}^{1+}$.

2 Theoretical Background

This chapter gives a theoretical overview of the physical principles used throughout this thesis. At first, the dominating decay channel in neutral $^{229\mathrm{m}}$Th, the so-called internal conversion decay, is described. This section aims to explain why the neutralization of $^{229(\mathrm{m})}$Th ions is of importance for the measurements towards a precise determination of the transition energy performed in our group. As the $^{229(\mathrm{m})}$Th ions used in the experiment will be guided by electric fields, the motion of charged particles in an electric potential is explained. Furthermore, the behaviour of ions that change their charge state in an electric field is deduced. In the experiment, this will be of importance for the charge exchange of thorium ions in carbon foils. Hereupon, the charge equilibrium that can be reached by ions penetrating through matter due to electron loss and capture is introduced in order to make predictions for the experiment. One of the materials penetrated by the thorium ions in the experiment is graphene. Therefore, a short introduction to the response of graphene to ion irradiation and its exceptional electric properties follows.

2.1 Thorium - Internal Conversion

The first excited nuclear state of ^{229}Th exhibits two main decay channels to the ground state: the radiative γ-decay and internal conversion (IC) [14].
In the IC-process, nucleus-shell coupling occurs: The excitation energy that is set free by the decay of the excited nuclear state gets transferred to an atomic shell electron via an electromagnetic interaction (virtual photon). Due to the gain of energy, the electron is ionized and emitted into the continuum. A Feynman diagram of the decay process via internal conversion is shown in Fig. 2.1.

Due to energy conservation, the kinetic energy E_e of the emitted electron equals to the difference between the electron's binding energy E_b and the nuclear transition energy E_γ:

$$E_\mathrm{e} = E_\gamma - E_\mathrm{b}. \tag{2.1}$$

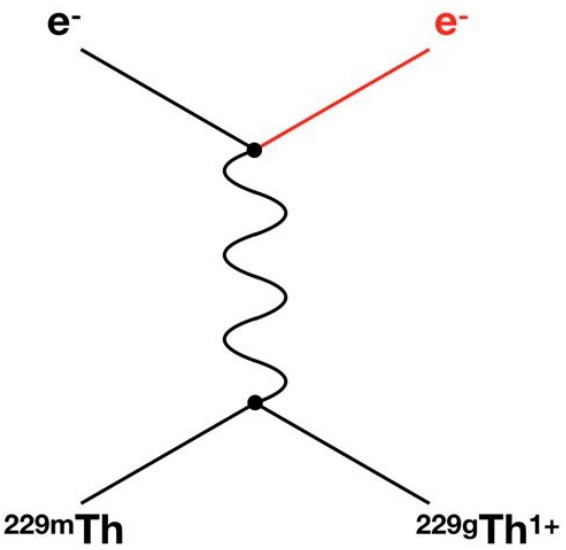

Figure 2.1: Feynman diagram of the isomeric decay via internal conversion in ^{229}Th: The excited nuclear state $^{229\mathrm{m}}$Th decays to the nuclear ground state $^{229\mathrm{g}}$Th, the excitation energy is transferred to an electron in the atomic shell, which is then emitted. The $^{229\mathrm{g}}$Th therefore ends up being singly charged.

The isomeric decay via internal conversion is thus conditioned by the electron's binding energy E_b being smaller than the nuclear transition energy E_γ:

$$E_\mathrm{b} < E_\gamma. \tag{2.2}$$

In ^{229}Th, the singly charged state has an ionization energy of 11.9 eV. As the isomeric excitation energy has an exceptionally low value of about 7.8 eV [11], internal conversion is already energetically forbidden in $^{229\mathrm{m}}\mathrm{Th}^{1+}$. This is why the predominant decay channel in thorium ions was expected to occur via γ decay, which is expected to have a lifetime of about 10^4 s.
A lifetime of $\tau > 1$ min has been confirmed in experiments [13], however, only for $^{229\mathrm{m}}\mathrm{Th}^{3+}$ and $^{229\mathrm{m}}\mathrm{Th}^{2+}$. The determination of the lifetime in $^{229\mathrm{m}}\mathrm{Th}^{1+}$ is still pending, but was already found to be shorter than 10 ms [15].

The lifetime of the isomer in neutral thorium atoms (first ionization potential of 6.3 eV), where IC is expected to be the dominant decay channel, was found to be $7 \pm 1\ \mu$s [15]. As a result of the different lifetimes of the isomer in neutral thorium and thorium ions, the decay via internal conversion can be triggered by neutralizing thorium ions.

2.2 Charged particles in an electric field

In this section, the motion of charged particles in a homogeneous electric field is described, the derivations are based on Ref. [16].

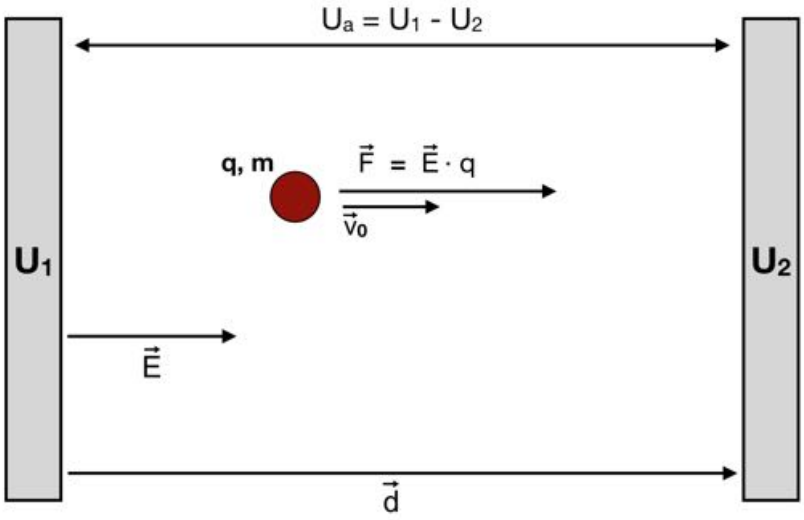

Figure 2.2: Charged particle in an electric field induced by two parallel electrodes, analogously to a plate capacitor.

Two plate electrodes are placed next to each other in a distance $\vec{d}$ ($d = |\vec{d}|$), arranged analogously to a parallel plate capacitor. Applying voltages U_1 and U_2 to those electrodes, a constant electric potential difference and thus an electric field is established. Implying the workfunctions (cf. Ref. [17]) W_1 and W_2 of the electrodes, the acceleration voltage can be defined as

$$U_\mathrm{a} = (U_1 + W_1) - (U_2 + W_2). \tag{2.3}$$

In the following, it will be assumed that the surfaces of the two electrodes have the same workfunctions, thus $W_1 = W_2$. Therefore, the accelerating voltage which affects any charged particle located between the two electrodes, can be defined as follows (see Fig. 2.2):

$$U_\mathrm{a} = U_1 - U_2. \tag{2.4}$$

The electric field equals

$$\vec{E} = \frac{U_\mathrm{a}}{d^2} \cdot \vec{d}. \tag{2.5}$$

A charged particle in this electric field is affected by the electric force

$$\vec{F} = \vec{E} \cdot q = \frac{U_\mathrm{a}}{d^2} \cdot \vec{d} \cdot q, \tag{2.6}$$

where q equals the charge of the particle (defined as to assign a value of $q = 1\mathrm{e}$ to a singly charged positive ion, $q = 2\mathrm{e}$ to a doubly charged positive ion etc.). This electric force leads to an acceleration of the charge carrier, which equals

$$\vec{a} = \frac{\vec{F}}{m} = \frac{\vec{E} \cdot q}{m}, \tag{2.7}$$

where $\frac{q}{m}$ is the specific charge, the ratio of the electric charge to the mass of a particle.

The work performed on the charged particle equals

$$W = \vec{F} \cdot \vec{d} = U_\mathrm{a} \cdot q. \tag{2.8}$$

This work increases the kinetic energy of the charged particle, therefore

$$E_\mathrm{kin} = \frac{1}{2} m \vec{v}^2 = U_\mathrm{a} \cdot q \tag{2.9}$$

which leads to the definition of the unit electronvolt [eV]:

The electronvolt (unit symbol: eV) is a unit often used in atomic, nuclear and particle physics. Since it will be used throughout this thesis, it is shortly described in the following:
By definition, an electronvolt is the energy that a particle possessing the charge 1 e (elementary electric charge) gains when moving through an electric potential difference of one Volt. In vacuum, it is thereby accelerated and obtains a gain in energy of

$$1\,\mathrm{eV} \approx 1.602 \cdot 10^{-19}\,\mathrm{J}. \tag{2.10}$$

In the case that the charged particle already possesses a kinetic energy when entering the electric field, the additional kinetic energy E_kin, caused by the electric potential difference, has to be added to the initial kinetic energy $E_0 = \frac{1}{2} m \vec{v}_0^2$ to obtain the total kinetic energy $E_\mathrm{kin}(tot)$ of the particle:

$$E_\mathrm{kin}(tot) = E_0 + E_\mathrm{kin}. \tag{2.11}$$

2.3 Behaviour of ions in electric fields undergoing charge exchange

In the experiment, positive ions with an initial charge q_{in} get accelerated towards a thin foil by a potential difference between a start potential (U_0) and the potential of the foil (U_{C}) with $U_0 > U_{\mathrm{C}}$. In the utilised carbon foil, the ions may capture or set free electrons and therefore leave the foil in a different charge state q_{exit}. The particles leaving the foil as neutral atoms ($q_{\mathrm{exit}} = 0$) can no longer be influenced by electric fields, whereas the exiting ions can be slowed down by a voltage difference between the foil and a ring electrode (blocking electrode), where $U_{\mathrm{C}} < U_{\mathrm{block}}$. Depending on the value of the blocking voltage applied, the ions can either pass the blocking electrode or be deflected. This process is depicted in stages ① - ④ in Fig. 2.3.

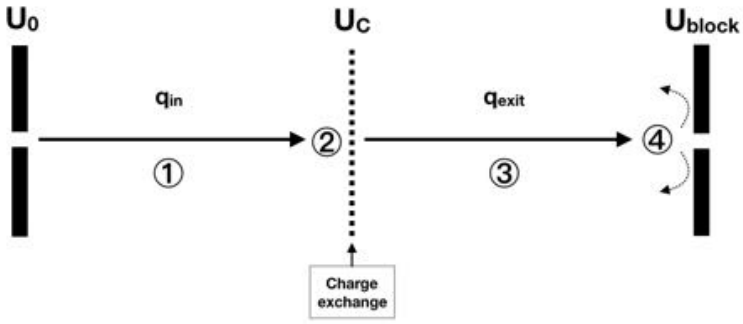

Figure 2.3: Scheme of an ion undergoing charge exchange in a foil.
①: A positively charged particle (q_{in}) is accelerated due to the voltage difference between an electrode (U_0) and the foil (U_{C}), with $U_0 > U_{\mathrm{C}}$.
②: The ion impinges onto the foil with a kinetic energy $E_{\mathrm{kin}}(\mathrm{foil})$ (Eq. (2.12)).
③: After leaving the foil, the exiting particle (now in the charge state q_{exit}) enters the electric field caused by the foil and the blocking electrode ($U_{\mathrm{C}} < U_{\mathrm{block}}$). The ions leaving the foil positively charged are thus slowed down, whereas the neutralized particles ($q_{\mathrm{exit}} = 0$) are not influenced.
④: Depending on the voltage applied to the blocking electrode, the ions can either pass through the hole in the electrode or will be deflected.

The kinetic energy of an ion at stage ② in the setup shown in Fig 2.3, so just before impinging onto the foil, can be determined by the following equation (cf. Eq. (2.9)):

$$E_{\mathrm{kin}}(\mathrm{foil}) = q_{\mathrm{in}} \cdot (U_0 - U_{\mathrm{C}}). \tag{2.12}$$

Under the condition that the ions reach the blocking electrode, their kinetic energy at the point of the blocking electrode is determined as

$$E_{\mathrm{kin}}(\mathrm{end}) = q_{\mathrm{in}} \cdot (U_0 - U_{\mathrm{C}}) + q_{\mathrm{exit}} \cdot (U_{\mathrm{C}} - U_{\mathrm{block}}). \tag{2.13}$$

For a certain value of the blocking potential U_{block}, the ions will no longer be able to pass the electrode. This limiting case is defined by the condition $E_{\mathrm{kin}}(\mathrm{end}) = 0$. For values of U_{block} larger than the limiting blocking voltage, the ions will no longer approach the electrode and instead be deflected. In the following, the minimum blocking voltage $U_{\mathrm{block,min}}$ which is required to deflect charged particles, is deduced using the condition $E_{\mathrm{kin}}(\mathrm{end}) = 0$:

$$E_{\mathrm{kin}}(\mathrm{end}) = 0 \tag{2.14}$$

$$\Rightarrow q_{\mathrm{in}} \cdot (U_0 - U_{\mathrm{C}}) + q_{\mathrm{exit}} \cdot (U_{\mathrm{C}} - U_{\mathrm{block,min}}) = 0 \tag{2.15}$$

$$\Rightarrow U_{\mathrm{block,min}} = \frac{q_{\mathrm{in}}}{q_{\mathrm{exit}}} \cdot (U_0 - U_{\mathrm{C}}) + U_{\mathrm{C}}. \tag{2.16}$$

A positively charged ion exiting the foil can therefore be blocked with a blocking voltage higher than a certain value, depending on its initial charge state q_{in}, its exiting charge state q_{exit} and the voltages U_0 and U_{C}.

The passage (stages ① - ③) of an ion through the potentials of the setup used in this thesis is illustrated in Fig. 2.4. The zero line was inserted to indicate its occurence in the experiment.

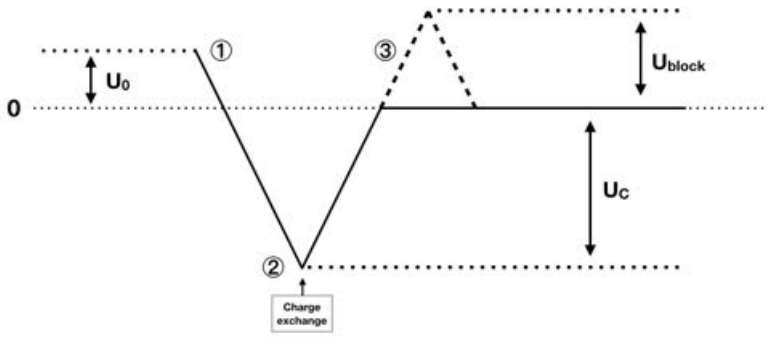

Figure 2.4: Scheme of the potential that an ion traverses in the setup of the experiment.
①: The ion starts off at a voltage $U_0 > 0$.
②: It is then accelerated towards the foil ($U_{\mathrm{C}} < 0$), where it can change its charge state ($q_{\mathrm{in}} \rightarrow q_{\mathrm{exit}}$).
③: The exiting ion can be blocked with a voltage $U_{\mathrm{block}} \geq U_{\mathrm{block,min}}$ (see Eq. (2.16)).

2.4 Charge equilibrium

The experiment is based on the occurrence of charge exchange of ions that pass through a thin carbon foil. In the following, it will be shown that the mean charge state of an ion penetrating a medium can be estimated. The explanations in this section follow Ref. [18].

It has been experimentally demonstrated that ions are capable of capturing an electron when colliding with an atom of the penetrated layer and therefore changing their charge state.
When decreasing the charge state of an ion, energy is set free, whereas to increase the charge state of an ion, energy is required. It may therefore be assumed that the cross section of electron capture increases with increasing ion charge. Conversely, this cross section will decrease with decreasing ion charge and rapidly go to zero for negative ions. As a result, the probability of a projectile to be in a certain charge state has a maximum near some equilibrium charge state and decreases monotonically in both directions. In the case that the initial charge is higher than the equilibrium charge, electron capture usually dominates over electron loss.
This means that a penetrating positive ion is able to capture electrons until it reaches the equilibrium charge state. Whether such an equilibrium state is actually achieved depends not only on the interaction time (thus on the thickness of the penetrated medium and the ion velocity) but also on the rate of energy loss.

The average of the resulting charge distribution is called the mean equilibrium charge and can be predicted using Bohr's stripping criterion.
It depends on the orbital velocities v_e of the electrons circling the nucleus and the velocity v of the ion itself. In the case that $v_\mathrm{e} < v$, the considered electron is only weakly bound and hence can easily be stripped off (ionization). Conversely, in the case of $v_\mathrm{e} > v$, the electron is likely to remain bound.
In the case of a positive ion, the outermost electrons will have large orbital velocities. This leads to the assumption that there are empty states in the atomic shell into which electrons can be captured. Therefore there must be an equilibrium where, considering a certain period of time, the number of electrons being split off equals on average the number of electrons being captured.

Making use of a definition by Niels Bohr (cf. [19]), the equilibrium charge state q_I can be approximated to the following:

$$q_\mathrm{I} = n\frac{v}{v_0} \tag{2.17}$$

where n denotes the principal quantum number of the outermost shell and $v_0 = \frac{c}{137}$ the Bohr velocity. The probability of a particle exiting the penetrated matter to be in a particular charge state will therefore have a maximum at this equilibrium charge state q_I.

Charge Equilibrium in $^{229(\mathrm{m})}\mathrm{Th}^{3+}$

In the experiment, mainly $^{229(\mathrm{m})}\mathrm{Th}^{3+}$ ions will be used as projectiles. Therefore their charge equilibrium will be calculated in the following.
The incoming $^{229(\mathrm{m})}\mathrm{Th}^{3+}$ ions have a kinetic energy $E_\mathrm{kin} \approx 2445\,\mathrm{eV}$ (following from Eq. (2.12) for $U_0 = 15\,\mathrm{V}$, $U_\mathrm{C} = -800\,\mathrm{V}$ and $q_\mathrm{in} = 3$), which corresponds to a velocity $v \approx 45400\,\frac{\mathrm{m}}{\mathrm{s}}$, and the principal quantum number is $n = 5$ for the outermost shell. Using those parameters in Eq. (2.17) leads to:

$$q_\mathrm{I}(^{229(\mathrm{m})}\mathrm{Th}^{3+}) \approx 5 \cdot \frac{45400\frac{\mathrm{m}}{\mathrm{s}}}{v_0} \approx 0.10. \tag{2.18}$$

A charge equilibrium of 0.10 means that most of the exiting particles are expected to be neutral atoms. Therefore most of the $^{229(\mathrm{m})}\mathrm{Th}^{3+}$ ions are expected to undergo neutralization when penetrating a thin carbon foil.

In order to reach a different charge equilibrium, the velocity v of the ions has to be adapted. By rearranging Eq. (2.17), the following can be found:

$$v = \frac{q_\mathrm{I} \cdot v_0}{n}. \tag{2.19}$$

For example, to generate mainly $^{229(\mathrm{m})}\mathrm{Th}^{1+}$ ions in the foil, an equilibrium charge of $q_\mathrm{I} \approx 1$ has to be reached. The velocity of the incoming $^{229(\mathrm{m})}\mathrm{Th}^{3+}$ ions to have such a charge equilibrium can be calculated:

$$v\,(q_\mathrm{I} = 1) = \frac{1 \cdot v_0}{5} \approx 4.4 \cdot 10^5\,\frac{\mathrm{m}}{\mathrm{s}}. \tag{2.20}$$

Based on the considerations above, it can be estimated that for a population of mainly $^{229(\mathrm{m})}\mathrm{Th}^{1+}$ ions a kinetic energy $E_\mathrm{kin} \approx 230\,\mathrm{keV}$ of the incoming $^{229(\mathrm{m})}\mathrm{Th}^{3+}$ ions is required. A high population of $^{229(\mathrm{m})}\mathrm{Th}^{1+}$ is essential for the measurement of the $^{229\mathrm{m}}\mathrm{Th}^{1+}$ lifetime.

2.5 Response of graphene to ion irradiation

In the experiment, the efficiency of the neutralization of ions in graphene is of particular interest. The description of the interaction between ions and graphene in this section follows Ref. [20].

Graphene consists of a single layer of carbon atoms and possesses exceptional electronic properties. One of them being an exceptionally high charge carrier density and mobility. This is the reason why it can be used to efficiently deliver electrons to positively charged ions for charge neutralization. The efficiency of the neutralization has been tested with highly charged ions (HCI), which were able to capture a large number of electrons during their passage through a single layer of graphene [20]. This is schematically shown in Fig. 2.5. With an increasing interaction time, the number of captured electrons is expected to rise. It has been found that due to the impact of the incoming ions, not only neutral or positively charged ions were emitted from the graphene, but also electrons. Therefore, in the experiment performed in this thesis it is essential to make sure that the electrons, emitted while thorium ions pass the graphene, are not misinterpreted.

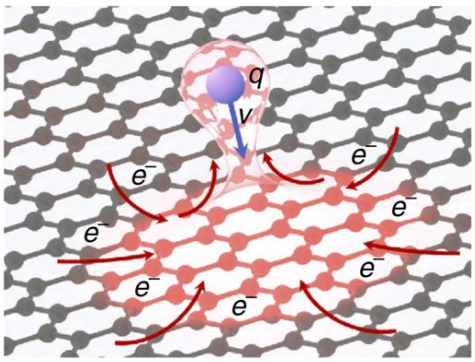

Figure 2.5: Interaction process between an approaching (highly charged) ion and graphene: Electrons moving freely in the graphene are captured by an impinging ion [20].

The vacancies generated with the capture of electrons by ions are promptly resupplied and the impact energy transferred to the graphene by the incoming ions is distributed due to the extraordinary electronic properties of graphene. A deformation of the graphene structure resulting from Coulomb explosion is hereby prevented. Therefore structural defects in graphene due to ion irradiation are not expected.

3 Experimental Setup

The aim of this thesis is to examine the charge exchange of thorium ions in carbon foils. Of particular interest are the efficiency for neutralization and the separation of the exiting charge states. Therefore, two experiments with different setups were performed, which are shown in Fig. 3.1 and Fig. 3.2. Both experiments consist of three parts: A $^{229(\mathrm{m})}$Th ion beam formation system (❶), a charge exchange setup (❷) and a detection system (❸). Each of the experimental components will be discussed in the following.

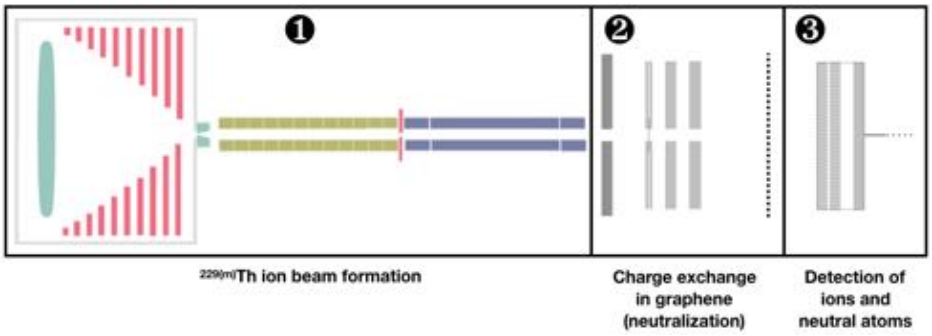

Figure 3.1: Conceptual scheme of the experimental setup used to test the efficiency of the neutralization of $^{229(\mathrm{m})}$Th ions in a graphene foil. See explanation in the text for details.

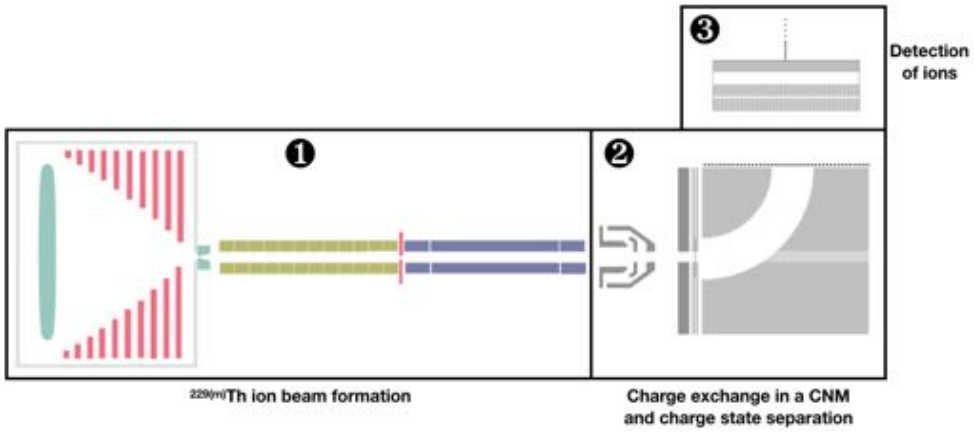

Figure 3.2: Conceptual scheme of the experimental setup used to separate the exiting particles according to their charge states. See explanation in the text for details.

At first, the setup for the formation of the $^{229(m)}$Th ion beam is explained, these ions can then be used as projectiles for both of the two experiments. Hereupon, the setups for examining the neutralization of $^{229(m)}$Th ions in a carbon foil and separating the exiting charge states using a curved plate capacitor are exemplified. Those setups can be attached to the ion beam formation part. A description of the MCP detection system and the signal readout follows.

Due to their availability at our experiment, in the first experiment (neutralization), a dual layered graphene foil was used, whereas in the second experiment (charge state separation) a carbon nano membrane was used as the penetrating matter in which charge exchange occurs. For both of them, high charge capture efficiencies during ion irradiation were observed. The most important difference between those two is that graphene is more stable. In a carbon nano membrane, because of its low electron mobility, Coulomb explosion can tear holes into the foil. However, in the experiment a degradation of the extraction of ions was not observed. In further considerations they will therefore be assumed to have equivalent properties concerning charge exchange.

3.1 $^{229(m)}$Th ion beam formation

The setup for the creation of a pure $^{229(m)}$Th ion beam consists of a system of vacuum chambers, where α-recoil ions originating from a radioactive source can be slowed down and accumulated in a bunch. The first chamber, the buffer-gas stopping cell, is filled with 30 mbar of ultrapure helium, which is used to stop the recoil ions. The ions are then guided by electric RF+DC fields towards an extraction nozzle and finally dragged by the emerging supersonic gas jet into an extraction vacuum chamber ($p \approx 5 \cdot 10^{-4}$ mbar), where short ion bunches are created in a segmented radiofrequency quadrupole ion guide (equivalent to a linear Paul trap). In the subsequent, separately pumped vacuum chamber ($p \approx 10^{-5}$ mbar), ions with a specific mass-to-charge ratio can be selected using a customized quadrupole mass spectrometer. A conceptual scheme of this setup can be seen in Fig. 3.3 and a realistic, 3-dimensional sketch is shown in Fig. 3.4. A detailed description is given in the following (cf. Ref. [14]):

$^{229(m)}$Th ions can be obtained via the α decay of ^{233}U. Therefore, a ^{233}U source is installed in the buffer-gas stopping cell for this experiment. The $^{229(m)}$Th ions and other α-recoil ions, which are mostly positively charged, leave the source with high kinetic energies and in all directions.
Collisions of the highly energetic ions with helium atoms contained in the buffer-gas stopping cell lead to a reduction of their velocities. A purity of helium in the ppb range is

necessary to make sure that the highly reactive thorium ions do not change their charge state or form various types of molecules.
An electric RF+DC funnel is used in order to lead the ions towards an extraction nozzle. The funnel system consists of ring electrodes arranged in the form of a cone. To reach an optimal ion extraction, RF and DC voltages are coupled and applied to the electrodes. The DC voltages follow a gradient, decreasing towards the exit of the funnel which accelerates the ions. The RF amplitude of neighboring electrodes is set to an alternating phase of 180° in order to prevent the ions from impinging onto them.

After passing through the extraction nozzle (in form of a Laval nozzle), the aim is to form an ion beam while removing the helium gas from the cell. Therefore, a radio-frequency quadrupole (RFQ) is installed, which consists of four segmented rods that are set to different voltages in order to stabilize the ions on the axis. The RF voltage of two opposing rods differs in phase by 180° compared to the other two rods, which leads to a radial confinement of the ions. The DC voltages can be applied to the segments individually and ensure that the ions are guided through the RFQ from one end to the other. Moreover, the residual helium gas pressure in the RFQ provides a phase-space cooling of the ion beam, thus improving its quality further.
The next-to-last segment of the RFQ is set to a voltage of U_0 = 15 V throughout the experiments. The DC offset of the last segment can be rapidly switched between two values. Applying a voltage higher than those of the other RFQ segments, a potential well can be created to temporarily trap the incoming ions. Switching the voltage to zero, those ions which accumulated at the last segment can be released at once. This system is used in order to create short ion bunches with a time-of-flight width of about 3 μs and a bunch rate of about 10 bunches per second. One single bunch includes about 400 $^{229(m)}Th^{3+}$ ions and about 320 $^{229(m)}Th^{2+}$ ions [15]. Only a minor part of $^{229(m)}Th^{1+}$ ions is extracted from the buffer-gas stopping cell [21]. While the ions are kept on a straight path, trapped and released, the helium gas can be removed by using a system of turbomolecular high vacuum pumps.

The ion beam leaving the RFQ still consists of all α-recoil ions leaving the ^{233}U source due to its decay chain. That is why in the next step, a quadrupole mass spectrometer (QMS) is used to select the thorium ions and remove all other ions in order to reduce the background produced by them. It consists of four stainless steel rods, to which RF and DC voltages can be applied. Choosing specific voltages, a certain mass-to-charge ratio can be selected to be transmitted across the QMS structure.

This setup allows to produce an almost pure thorium ion beam at low energies, partially

(~2%) being in the isomeric excited state ^{229m}Th, which can be used in further experiments.

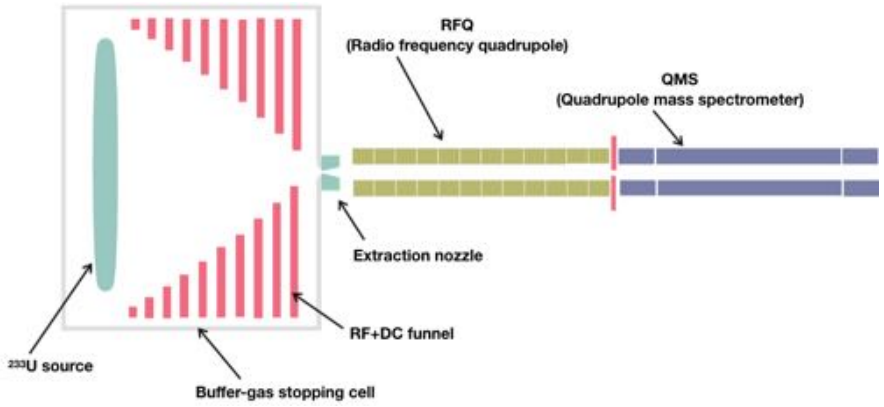

Figure 3.3: Conceptual scheme of the $^{229(m)}$Th ion beam formation system [14]. The ^{233}U source used for $^{229(m)}$Th α-recoil ion production is installed in the buffer-gas stopping cell. The helium buffer-gas contained inside slows down the ions, which are guided to the exit of the stopping cell by an RF+DC funnel. The ions are then injected into a radio frequency quadrupole (RFQ), where the ion beam is formed and can be bunched. Subsequently, they are purified using a quadrupole mass spectrometer (QMS). The dimensions are not to scale, since some of the electrodes were enlarged for better visibility. This ion beam is used as a basis for the experiments performed in this thesis.

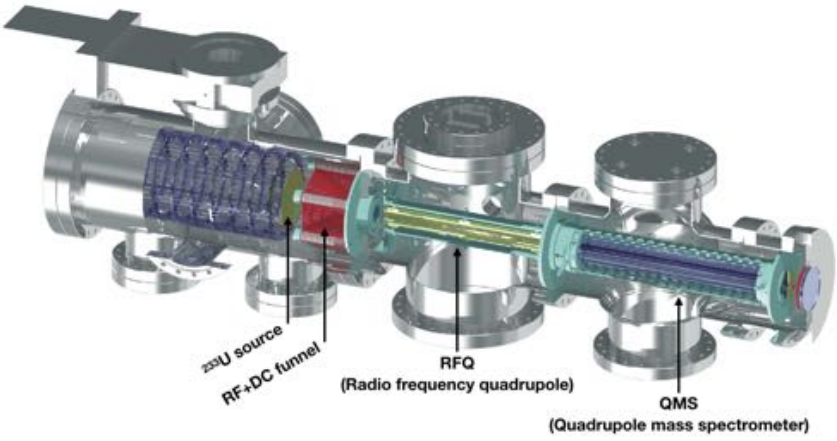

Figure 3.4: 3-dimensional sketch of the setup used for the formation of a clean $^{229(m)}$Th ion beam [14]. A detailed description is given in the text.

3.2 Charge exchange of $^{229(m)}$Th ions in graphene

At first, the efficiency of the carbon foil for neutralizing thorium ions has to be investigated. In this experiment, $^{229(m)}Th^{3+}$ ions (selected with the QMS) are sent through a graphene foil where charge exchange occurs.

As shown in Fig. 3.5, the ions are pulled towards the graphene by an electric force generated by applying a negative voltage to the focusing electrode (typical value: -2 V) and the graphene (between -300 V and -3000 V).

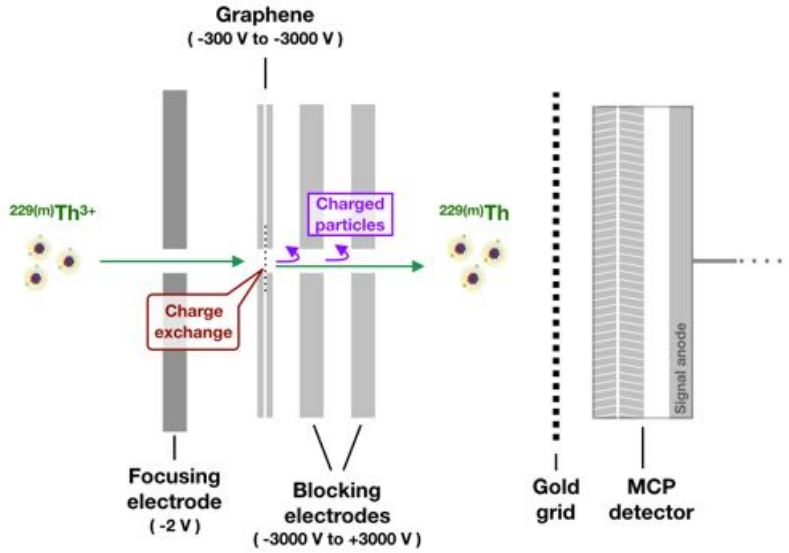

Figure 3.5: Scheme of the experimental setup used for the investigation of the neutralization of thorium ions in graphene. $^{229(m)}Th^{3+}$ ions are guided, by the focusing electrode, onto the graphene foil where charge exchange occurs. The exiting charged particles (but not the neutralized atoms) can be repelled by a voltage chosen high enough applied to the blocking electrodes. The particles exiting the setup can be examined with an MCP detector.

However, not only neutral $^{229(m)}$Th will be generated at the graphene, but also freely moving positive and negative ions as well as electrons set free due to the impact of the incoming ions.

To distinguish between the exiting particles, two blocking electrodes are installed behind the graphene foil, which can each be set to an either negative or positive voltage (between -3000 V and +3000 V). The minimum blocking voltages $U_{\mathrm{block,min}}$ required to block certain exiting charge states can be approximated via Eq. (2.16). By applying high enough blocking voltages, it is expected that positively and negatively charged particles are repelled and only neutral particles are detected at the MCP detector. A gold grid is placed in about 1 cm

distance from the MCP and in about 3-4 cm distance from the second blocking electrode and serves for shielding the electric field of the MCP from influencing the electric field induced by the blocking electrodes. For a detailed explanation of the MCP and the signal readout, see Sect. 3.4. Analyzing the exiting particles, the efficiency of using graphene for neutralizing thorium ions can be investigated.

Graphene can be produced in single atomic layers. The one used in the experiment is an EM-Tec dual layer graphene TEM support film, deposited on lacey carbon and supported by 300 mesh copper grids (provided by Micro to Nano - Innovative Microscopy Supplies). The indication of size of 300 mesh approximately corresponds to 300 holes per inch (25.4 mm). In this case, the grid is known to have a hole width of 54 μm and a grid width of 31 μm [22]. Lacey carbon is a carbon film that has a fine lacey structure which offers a great percentage of open area.

A photograph of the experimental setup is shown in Fig. 3.6. The holes in the blocking electrodes and the metal plates, which hold the graphene foil, have a diameter of about 3 mm, which corresponds to the diameter of the graphene foil.

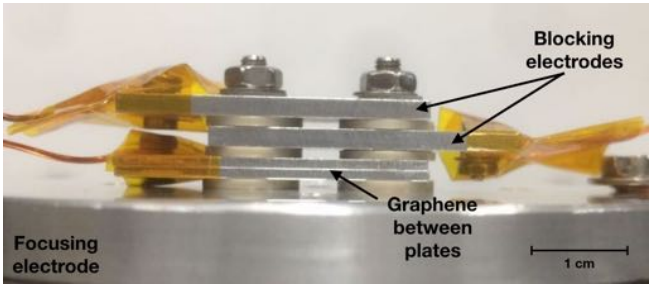

Figure 3.6: Photograph of the experimental setup, including the focusing electrode, the graphene foil (mounted between two plates) and the blocking electrodes.

The appearance of the graphene foil that was used in the experiments is examined with a microscope (Zeiss Axio Scope.A1) and compared to an unused one in order to investigate eventually occuring modifications due to the exposure to the ion irradiation. The results are shown in Fig. 3.7.

Some holes in the grid of the graphene foil, after having been irradiated in the experiment, do not show the spiderweb pattern of the pristine lacey carbon, therefore it must be concluded that in those regions also the graphene layer lost its integrity. In comparsion, however, the unused foil has an intact lacey carbon pattern in nearly all of the grid holes. This observation leads to the conclusion, that the holes in the foil were created during the experiment, for example by uncontrolled voltage sparks. As this applies only to a minor part of the grid

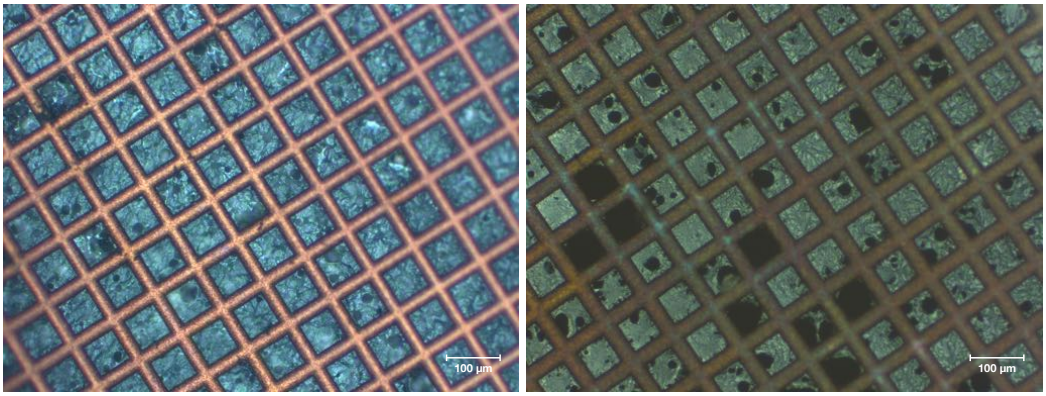

Figure 3.7: Microscopic snapshots (10x magnification) of the dual layer graphene film on Lacey Carbon and a 300 mesh copper grid (hole: 54 μm, bar: 31 μm) that was used in the experiment, unused (left) and used (right). Microscope: Zeiss Axio Scope.A1. Thanks to Anna Seiler and AG Weitz (LMU).

holes (regarding the whole graphene foil, not only the detail shown in Fig. 3.7), and did not remarkably change the count rates in the experiment, it can be considered as a minor impairment. However, it has to be assumed that a considerable part of the incoming $^{229(m)}Th^{3+}$ ions will be able to traverse the graphene foil through holes without changing their charge state. Those have to be reliably repelled by the blocking electrodes in order to detect only neutral atoms at the MCP detector.

In Fig. 3.8, microscopic close-ups of an intact and a defective grid hole are shown.

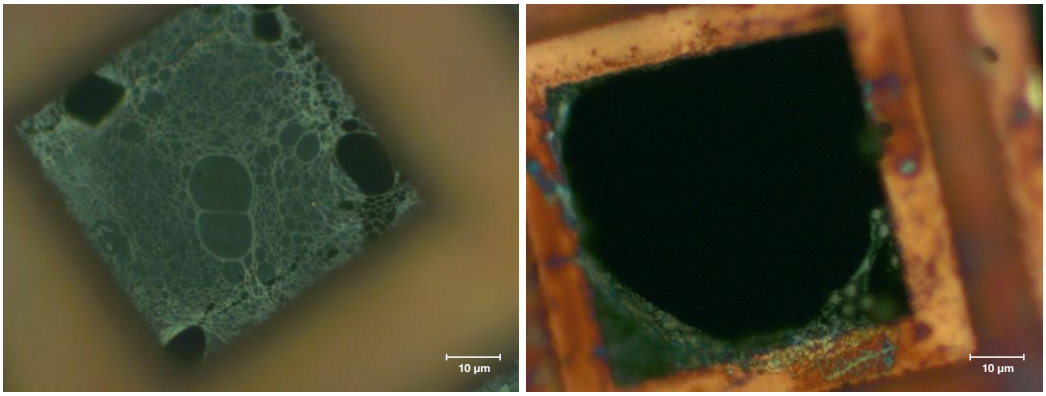

Figure 3.8: Microscopic close-ups (100x magnification) of an intact grid hole (left) and a defective one (right). Microscope: Zeiss Axio Scope.A1. Thanks to Anna Seiler and AG Weitz (LMU).

3.3 Charge state separation

The aim of this experiment is to analyze the particles that are generated by sending thorium ions through a carbon foil according to their charge state. A scheme of the setup can be seen in Fig. 3.9.

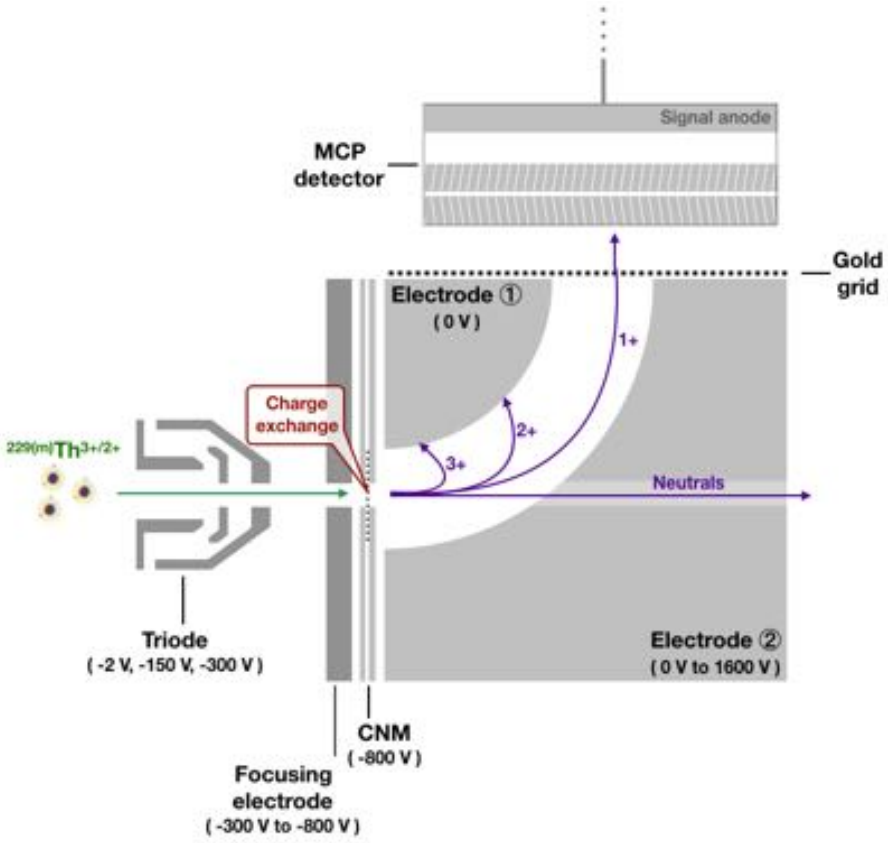

Figure 3.9: Scheme of the experimental setup used for charge state separation with the help of a curved plate capacitor. The incoming thorium ions are, by the triode and the focusing electrode, guided onto the carbon nano membrane (CNM) in which charge exchange occurs. The exiting particles are then led into the subsequent curved plate capacitor, where they can be separated according to their charge state due to an electric field applied. The particles which are able to exit the curved plate capacitor are detected at the MCP detector.

A triodic electrode structure, which was already built for prior experiments [14], is used as an ion guiding and focusing system. It consists of three electric apertures, to which different voltages (typical values: -2 V, -150 V, -300 V) can be applied in order to guide and focus the ions. Behind the triode, there is another electrode with a hole, through which the ions can pass. Applying a certain voltage (between -300 V and -800 V) to this electrode makes sure

that the ions extracted from the triode are focused onto the subsequently positioned carbon nano membrane (CNM). In the following, it will therefore be called the focusing electrode. The CNM (typical voltage: -800 V) used in this experiment is of the type Quantifoil Multi-A on a 300 mesh (~300 holes per inch) copper grid (provided by CNM Technologies Bielefeld) and was mounted between two metallic plates. The curved plate capacitor, made from aluminum, is the device where the exiting ions can be separated by their charge state. It consists of two curved electrodes to which different voltages are applied in order to achieve transmission dependent on the charge state. In the experiment, electrode 1 is set to 0 V whereas electrode 2 is varied between 0 V and 1600 V. In electrode 2, a cylindrical bore (5 mm diameter) was drilled in the direction of the particle beam in order to let the neutral atoms, which are not influenced by the electric field, leave the capacitor without generating secondary particles (e.g. electrons). The gold grid fixed to the exit of the curved plate capacitor serves for shielding the electric field of the MCP from influencing the deflection at the electrodes.

The dimensions of the curved plate capacitor are depicted in Fig. 3.10 and photographs of the side view and top view are shown in Fig. 3.11. A detailed explanation of the functionality of the multichannel plate detector (MCP) used for the detection of the exiting particles can be found in Sect. 3.4.

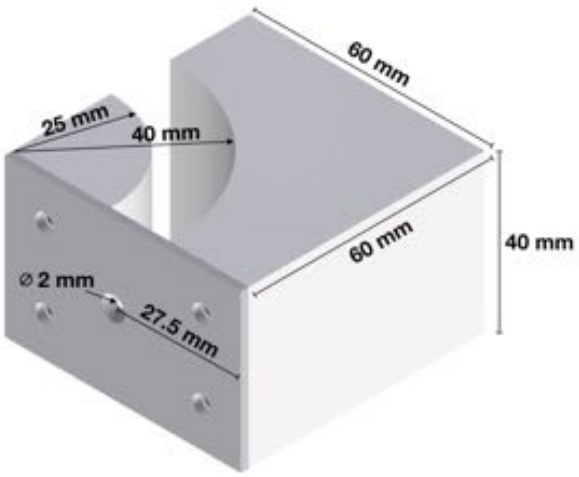

Figure 3.10: Drawing of the curved plate capacitor with dimensions. See text for details.

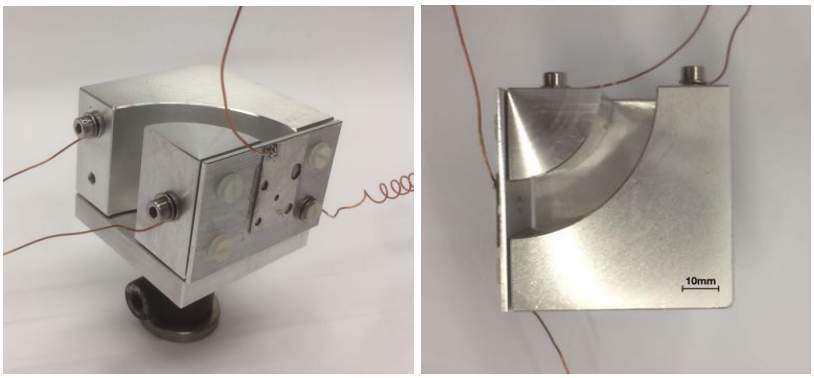

Figure 3.11: Photographs of the curved plate capacitor used for charge state separation, side view (left) and top view (right).

3.4 MCP detection system and signal readout

MCP Detection System

For particle detection in our experiments, a multichannel plate detector (MCP) in Chevron geometry is used (Model: Hamamatsu F-2223 [23]). MCPs are generally able to detect any charged particles and photons [24], but also neutral species [23]. In the two experiments described above, it will mainly be used to detect positively charged ions and neutral atoms.

The MCP detector consists of two plates (front and rear) that have microscopically small channels (~12 μm diameter [23]) and a consecutive anode, where the signal is detected. Three different voltages can be applied to the MCP: one to the front plate, one to the rear plate and another one to the signal anode. For the major part of the experiments, the voltage of the MCP front plate is set to -2000 V and the rear plate is connected to ground via a 5MΩ resistor. The signal anode is set to 0 V. For some experiments a voltage of -1800 V is applied to the front plate, the rear plate is set to ground (without the 5MΩ resistor). In this case, a voltage of 200 V is applied to the signal anode. The open area ratio (OAR) of the utilised MCP, which indicates the ratio of the channel open area to the entire surface of the MCP, amounts to ~ 60 % [23].

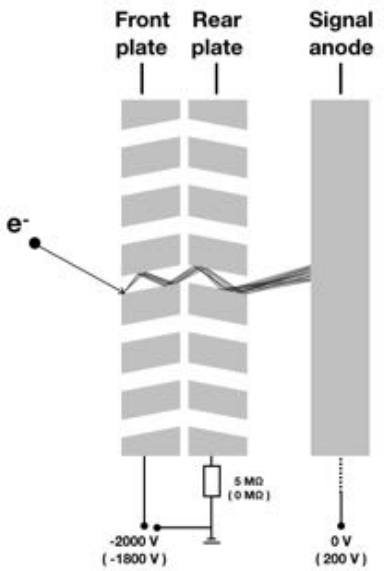

Figure 3.12: Conceptual scheme of the MCP's operational principle. The MCP can detect any event that triggers the emission of an electron on the MCP's surface. This electron is multiplied in one of the microchannels and can be detected as an electron shower at the signal anode. Typical voltage settings are indicated.

The operational principle of the MCP is illustrated in Fig. 3.12 and will be explained in the following:
An impinging particle can only be detected if it possesses an energy high enough to liberate electrons on the front surface of the MCP. If the impact of a particle on the surface of the MCP triggers the emission of an electron in one of the microchannels, this electron can set free secondary electrons by hitting the channel walls. In the experiment, a certain voltage difference (as seen in Fig. 3.12) will be applied between the two microchannel plates and the anode to create a potential that pulls occuring electrons towards the signal anode. More and more electrons will be set free as the electrons are accelerated towards the end of the channel. An electron avalanche will build up, which will be measureable at the signal anode. As a result, the signal of a single impinging particle is intensified by a factor of about 10^6 by the emission of multiple secondary electrons [24].

According to Ref. [25], an MCP can detect particular particle species like ions or neutral atoms with a decent quantum efficiency (QE). The following proportionality applies for the MCP detection efficiency for neutral particles and ions:

$$\epsilon_{\text{det}} \propto \frac{E}{\sqrt{m}}, \tag{3.1}$$

where E is the impact energy of the detected particle in keV and m equals to the mass of the particle in atomic mass units (u).

The OAR-limited maximum (60 %) of the QE is achieved for $\frac{E}{\sqrt{m}} > 1$. With a decrease of this value, the QE diminishes. The detection efficiency of the MCP detector is therefore approximated to

$$\epsilon_{\text{det}} \approx 0.6 \cdot \frac{E}{\sqrt{m}}. \tag{3.2}$$

Signal Readout

Signals from the MCP's signal anode are first preamplified by an ORTEC VT 120 preamplifier (modified by the LMU electronic workshop) and then amplified by an ORTEC 571 main (shaping) amplifier. The amplified signal is fed into a Constant Fraction Discriminator (CFD) of the type CFT 1300 (LMU). The device used for data acquisition (DAQ) is a PCI 6602 data card (provided by National Instruments) plugged into a PC, the recorded data can then be displayed. This process is depicted in Fig. 3.13.

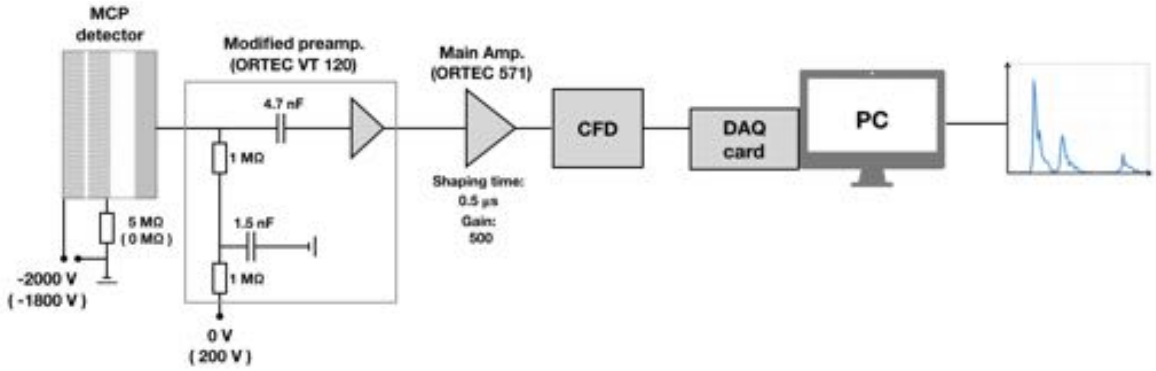

Figure 3.13: Block diagram of the experiment's signal readout: The signal from the MCP is intensified by a modified preamplifier, followed by a shaping amplifier. It is then fed into a Constant Fraction Discriminator (CFD) and afterwards into the data acquisition card (DAQ card). The data can then be displayed on the PC.

4 Results: Simulations and Measurements

4.1 Measurement goals

In the experiments discussed in this thesis, accelerated $^{229(\mathrm{m})}$Th ions are sent onto carbon foils. The main goal of the measurements is to show that the thorium ions can be efficiently neutralized by sending them through a carbon foil like graphene. This step is an important aspect of the experiments towards a precise measurement of the isomeric excitation energy of ^{229}Th performed in our group.
Another expectation is to not only detect neutral thorium atoms exiting the setup, but also a small fraction being singly charged ($^{229(\mathrm{m})}\mathrm{Th}^{1+}$).
This charge state is important, as a lifetime measurement of the excited nucleus in the singly charged thorium ion is still pending. The determination of this value is awaited for various envisaged experiments (e.g. Ref. [26]) and to potentially provide an explanation for the non-observation of an internal conversion decay signal from the thorium isomer in Ref. [13]. Therefore another important achievement is to clearly identify the singly charged thorium ions and separate them from the other charge states for further experiments.

4.2 Neutralization of $^{229(\mathrm{m})}$Th ions in graphene

For the following measurements, the setup shown in Fig. 3.1 is used. The variable part used in this experiment is depicted in more detail in Fig. 3.5, where also the arrangement of the electrodes is shown.

In order to change the kinetic energy of the ions that pass through the graphene layer, different voltages are applied to the foil. The voltages at the blocking electrodes can also be varied to enable an extraction of only neutral thorium atoms. In order to allow for this, one electrode has to be set to a negative voltage at least as high as the voltage applied to the graphene in order to deflect any electrons set free at it. The electrons set free at the potential

of the graphene are physically not allowed to overcome this potential, as long as there is no gain in energy. A positive voltage applied to a second electrode can regulate the blocking of positive ions. The triply charged ions can already be blocked with a low voltage, whereas the blocking of the singly charged state requires a higher voltage. The values of the voltages that successfully block the singly and double charged states depend on the voltage applied to the graphene foil, as it influences the kinetic energy of the particles and can be calculated using Eq. (2.16).

For this part of the experiment, the setting of the QMS was chosen as to only extract thorium ions in the triply charged state. The measurements were taken in the bunch mode explained in Sect. 3.1. The voltage applied to the focusing electrode was kept at -2 V throughout this part of the experiment and a voltage of -900 V was applied to the graphene foil. The voltage of the front plate of the MCP was set to -2000 V. Due to those settings, electrons set free at the graphene foil are energetically not allowed to reach the MCP. Therefore, no negative voltage has to be applied to one of the blocking electrodes in order to block negatively charged particles. Both blocking electrodes are short-circuited and thus both set to a positive voltage, which is varied throughout the experiment. For a voltage $U_0 = 15\,\mathrm{V}$, the minimum blocking voltages calculated in the following (using Eq. (2.16)) should be sufficient to successfully deflect the positively charged particles:

$$U_{\mathrm{block,min}}(3+ \rightarrow 3+) = 15\,\mathrm{V}, \tag{4.1}$$

$$U_{\mathrm{block,min}}(3+ \rightarrow 2+) = 472.5\,\mathrm{V}, \tag{4.2}$$

$$U_{\mathrm{block,min}}(3+ \rightarrow 1+) = 1845\,\mathrm{V}. \tag{4.3}$$

Considering the values obtained above, the detected signals at the MCP for different values of U_{block} were compared. Fig. 4.1 shows the time-of-flight spectra that were measured with different blocking voltages.

For low voltages applied to the blocking electrodes (see Fig. 3.5), two peaks are detected. Increasing the voltage, one of the peaks disappears. This means that the ions that were transmitted without changing their charge state or the ones that changed their charge state, but did not achieve neutralization, can be blocked by a positive voltage (chosen high enough) applied to one of the blocking electrodes. As it was expected, any peak originating from positive ions can be blocked for a voltage of 2000 V applied to the blocking electrodes, whereas the peak on the left side is not influenced by any voltage, which leads to the conclusion that they are neutral atoms.

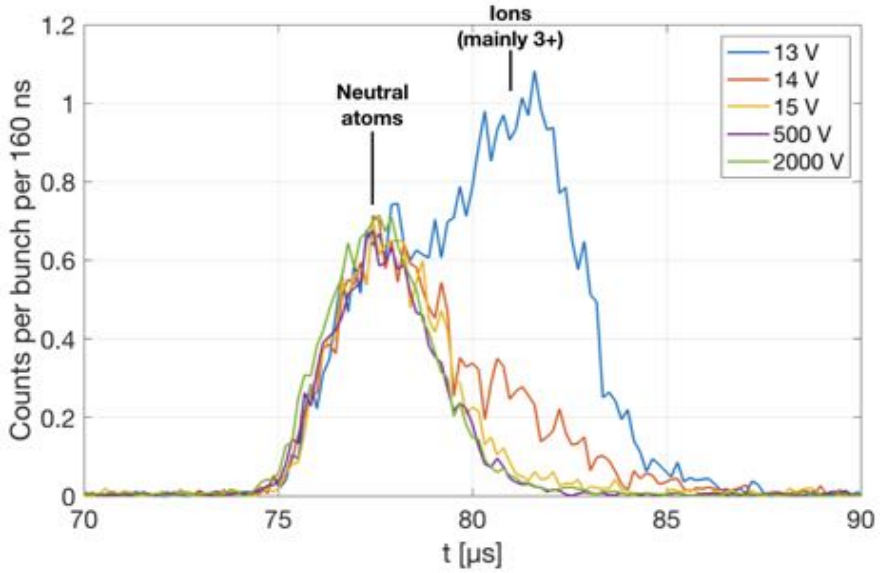

Figure 4.1: Time-of-flight spectrum of the particles exiting the setup, measured with the MCP detector for different blocking voltages U_{block}. The shown data is based on the detection of 500 bunches for values of U_{block} = 13 V, 14 V, 15 V and 1000 bunches for values of U_{block} = 500 V, 2000 V.

It has to be remarked that there is no sizeable count-rate difference between a voltage of 15 V to 2000 V applied to the blocking electrodes. This means that the positive ions that were blocked are mainly $^{229(m)}\mathrm{Th}^{3+}$ and that signals originating from $^{229(m)}\mathrm{Th}^{2+}$ ions or $^{229(m)}\mathrm{Th}^{1+}$ ions are not observed.

The temporal separation of the two peaks (the left one originating from neutral species, the right one from ions) is expected and is understood as follows:
The ions being in a positively charged state are attracted by the graphene foil and for this reason lose kinetic energy after having passed the graphene layer. Thus they reach the MCP detector at a later time than the neutral atoms, which are not decelerated after having passed the graphene foil. The initial energy E_0 of the $^{229(m)}\mathrm{Th}^{3+}$ ions that impinge onto the graphene foil equals to 45 eV (U_0 = 15 V). Using Eq. (2.13), the kinetic energies of the exiting particles, depending on their final charge state q_{exit}, can be calculated for $U_{\mathrm{block}} = 0\,\mathrm{V}$:

$$E_{\mathrm{kin}}(3+ \rightarrow 0+) = 2745\,\mathrm{eV}, \tag{4.4}$$

$$E_{\mathrm{kin}}(3+ \rightarrow 1+) = 1845\,\mathrm{eV}, \tag{4.5}$$

$$E_{\mathrm{kin}}(3+ \rightarrow 2+) = 945\,\mathrm{eV}, \tag{4.6}$$

$$E_{\mathrm{kin}}(3+ \rightarrow 3+) = 45\,\mathrm{eV}. \tag{4.7}$$

In the case of a positive voltage applied to the blocking electrode, the positive ions are further decelerated. The highly negative voltage (-2000 V) at the MCP does not have much of an impact on the kinetic energy of the charged particles, as it is shielded with a gold grid that is set to ground (see Fig. 3.5). The acceleration of the positive ions towards the MCP at this short distance can therefore be ignored. This allows for a temporal separation of the signals detected from neutral atoms and ions.

The occurence of $^{229(m)}Th^{3+}$ ions behind the graphene foil can be explained by the previously described holes in the graphene layer (see Fig. 3.7). The ions can traverse the holes without interacting with the graphene, thus without changing their charge state.
The measurements conducted above show that the largest fraction of the incoming $^{229(m)}Th^{3+}$ ions are neutralized when they pass through the graphene foil. For a quantitative analysis of the neutralization efficiency see Sect. 4.4.1.

Influence of the graphene voltage on the MCP count rate

The voltage applied to the graphene foil directly influences the amount of counts measured by the MCP detector. The measurements were performed with two different MCP settings (see Sect. 3.4). Different negative voltages (varying from -300 V to -3000 V) were then applied to the graphene layer and the first blocking electrode (short-circuited) in the same series of measurements. The number of counts in the region of interest (72 to 88 μs) were recorded. The voltage applied to the focusing electrode was kept at -2 V throughout this part of the experiment, whereas the second blocking electrode was kept at 200 V as to ensure that no $^{229(m)}Th^{3+}$ ions would be able to reach the MCP and cause a signal. The results for a voltage of the front plate of the MCP set to -2000 V and to -1800 V, respectively, are displayed in Fig. 4.2.

The linear increase of counts on the MCP, which was fitted into Fig. 4.2, can potentially be explained by a linear increase of the MCP detection efficiency. It is known from theory that the MCP detection efficiency is proportional to the kinetic energy of the neutral atoms [25]. For an increasing (negative) voltage U_C applied to the graphene layer, the kinetic energies of the neutral thorium atoms leaving the graphene foil increases as can be calculated with Eq. (2.13):

$$E_{kin}(3+ \rightarrow 0+,\, U_C = -1000\,\mathrm{V}) = 3045\,\mathrm{eV}, \tag{4.8}$$

$$E_{kin}(3+ \rightarrow 0+,\, U_C = -2000\,\mathrm{V}) = 6045\,\mathrm{eV}, \tag{4.9}$$

$$E_{kin}(3+ \rightarrow 0+,\, U_C = -3000\,\mathrm{V}) = 9045\,\mathrm{eV}. \tag{4.10}$$

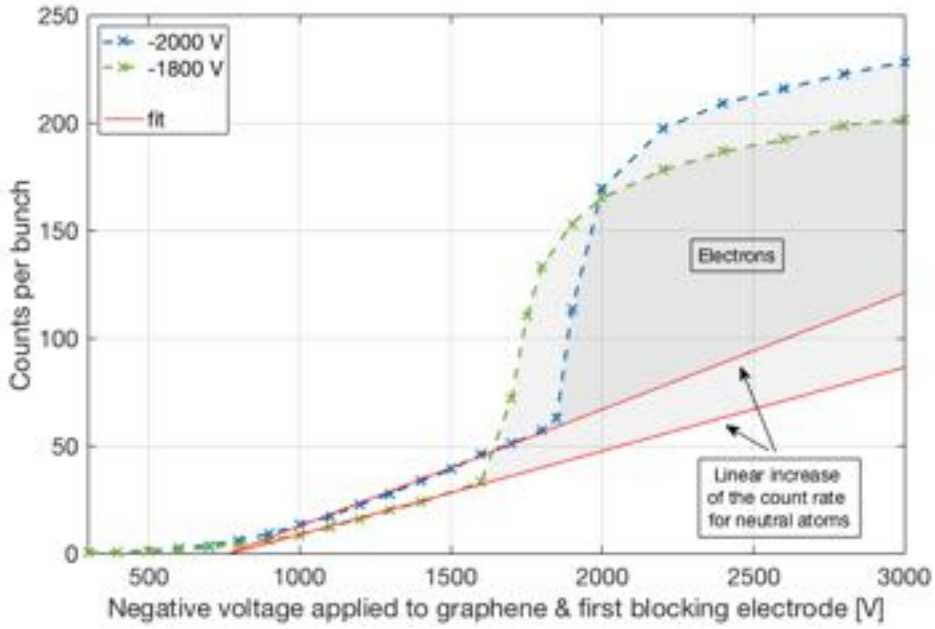

Figure 4.2: Influence of the voltage applied to the graphene foil (and the first blocking electrode) on the count rate detected at the MCP, examined for voltages of -2000 V and -1800 V, respectively, applied to the front plate of the MCP. The shown data is based on the detection of 1000 bunches per measurement point. The error bars are smaller than the symbols.

At this point it should be remarked that a higher voltage applied to the graphene foil can also lead to an enhanced focusing effect and therefore to an increase of the number of neutral atoms detected at the MCP. However, it is assumed that the main reason for this linear increase is the increasing detection efficiency of the MCP for higher kinetic energies.

An additional, steplike increase of counts is observed at a graphene voltage of -1850 V for an MCP voltage of -2000 V and of -1600 V for an MCP voltage of -1800 V, respectively. This is due to electrons generated at the graphene during the ionic impact, being energetically able to reach the MCP from that point on. The recorded counts that can be assigned to electrons in the measurements above (Fig. 4.2) are shown in Fig. 4.3.

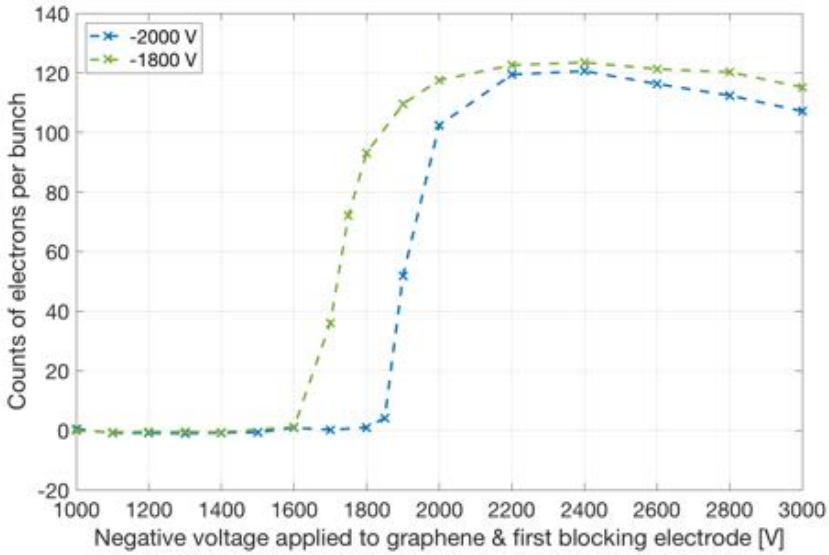

Figure 4.3: Influence of the voltage applied to the graphene foil (and the first blocking electrode) on the detection of electrons at the MCP, examined for voltages of -2000 V and -1800 V applied to the front plate of the MCP. The shown data is based on the detection of 1000 bunches per measurement point. The error bars are smaller than the symbols.

4.3 Charge state separation

From the measurements described in the previous section, it is obvious that neutralization occurs. However, the setup cannot be used for exit charge-state analysis. Therefore, a second experiment that allows for charge state separation using a curved plate capacitor is performed.

4.3.1 Simulations

The ion optics simulator SIMION 8.1 [27] was used to test the performance of the curved plate capacitor. The geometry of this capacitor in the simulations and an example of the ion trajectories is depicted in Fig. 4.4.

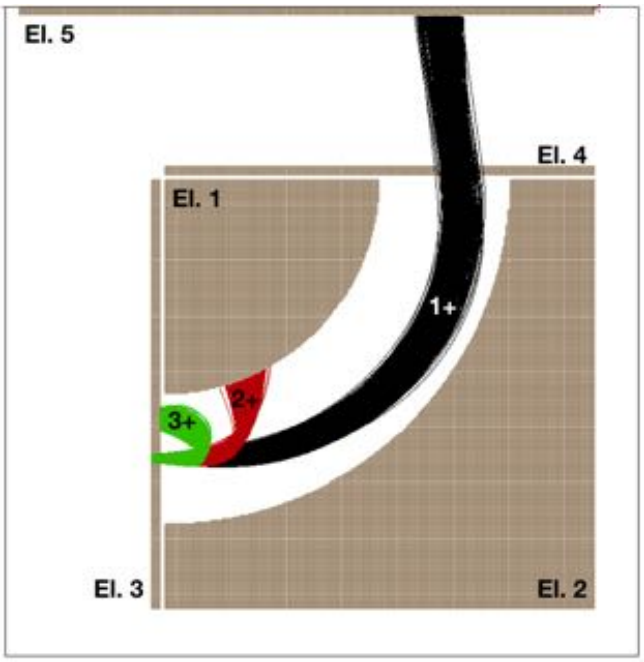

Figure 4.4: Screenshot taken from the SIMION simulations that shows the geometry used for the ion trajectory simulation. An example for the trajectories of different exit charge states is shown. In the present case, the 1+ charge state is transmitted (thus the voltage of electrode 2 being between ~ 800 V and ~ 1400 V). In this example, all of the charge states have a kinetic energy of 2.4 keV at the starting point at electrode 3, which is set to -800 V.

The electrodes labeled with the numbers 1 to 5 can be set to different voltages. The starting point of the simulated particle trajectories is at electrode 3. For the kinetic energy of the

particles at the starting point applies that $E_{\mathrm{kin}} = q_{\mathrm{in}} \cdot U_{\mathrm{C}}$. In the simulation, U_{C} equals to the voltage applied to electrode 3. Thus, all particles originating from one certain initial charge state q_{in} will start off with the same kinetic energy for a constant voltage applied to electrode 3. The direction of the particles is set to follow a filled cone distribution with an opening angle of 10 degrees. In order to separate the charge states, only a positive voltage will be applied to electrode 2 instead of applying also a negative voltage to electrode 1. This was proven to not make a great difference in the distinction of the charge states and is easier applicable in the experiment.

Variation of the voltage applied to the curved plate capacitor (El.2)

In the simulation, -800 V were applied to electrode 3 which will, in the experiment, correspond to the carbon nano membrane (CNM). Using Eq. (2.9), this leads to a kinetic energy of 2.4 keV for the 3+ ions and 1.6 keV for the 2+ ions entering the CNM. This means, that the particles originating from a certain initial charge state q_{in} will start off with the same kinetic energy but will, dependent on their exit charge state, be slowed down by their attraction to the negative voltage applied to electrode 3. They can therefore be distinguished by their kinetic energies. The voltage applied to the charge state separator (to electrode 2) was varied from 0 V to 1400 V for both of the initial kinetic energies. The particles are counted when the particles are able to exit the curved plate capacitor and reach electrode 5.

The results of the simulation obtained with the parameters described above are shown in Fig. 4.5.

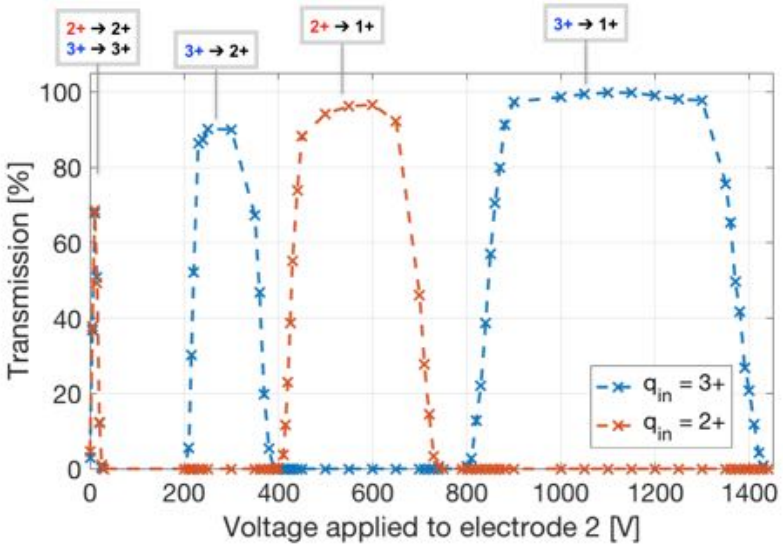

Figure 4.5: Simulation of the charge state separation: Variation of the voltage at electrode 2. The transmission shown in this graph is normalized for each pair of $q_{\mathrm{in}} \rightarrow q_{\mathrm{out}}$.

The ions possessing the same charge state before and after passing the CNM (3+ ions with 2.4 keV and 2+ ions with 1.6 keV) can easily be influenced by the electric potential generated by the voltage applied to the charge state separator. Therefore they leave the capacitor and will be detected at a low voltage of about 0 V to 30 V.
A higher voltage is required to influence the 2+ ions originating from the 3+ charge state (thus having an energy of 2.4 keV). They can be made visible at the detector at a voltage of between about 200 V and 400 V. An even higher voltage of between about 400 V to 750 V is needed to detect the 1+ ions originating from the 2+ charge state (thus having 1.6 keV of kinetic energy). In order to make 1+ ions, originating from the 3+ charge state (2.4 keV), leave through the exit hole in the capacitor, a voltage of about 800 V to 1450 V is needed. As a result, a clear distinction of the charge states is possible in simulations.

Behaviour of the charge state separation for different kinetic energies

In Fig. 4.6 the influence of the voltage applied to the CNM (electrode 3) is simulated.
When increasing the voltage by steps of 100 V, it is evident, that the voltage that has to be applied to electrode 2, to make the maximum number of ions leave the CNM in the singly charged state, also increases. As a result, it can be assumed that for an increasing voltage applied to the CNM, a higher voltage has to be applied to electrode 2 in order to reach a maximum of transmission. This is consistent with expectations, as for particles having a higher kinetic energy (with the increase of the voltage applied to the CNM) a higher voltage at electrode 2 is needed to deflect them. However, the voltage that has to be applied to make the maximum number of 2+ turning into 1+ reach the detector, increases only half as much as the voltage required to make the maximum number of 3+ turning into 1+ visible on the detector. This can be explained with the 2+ incoming ions having a lower kinetic energy than the 3+ incoming ions.

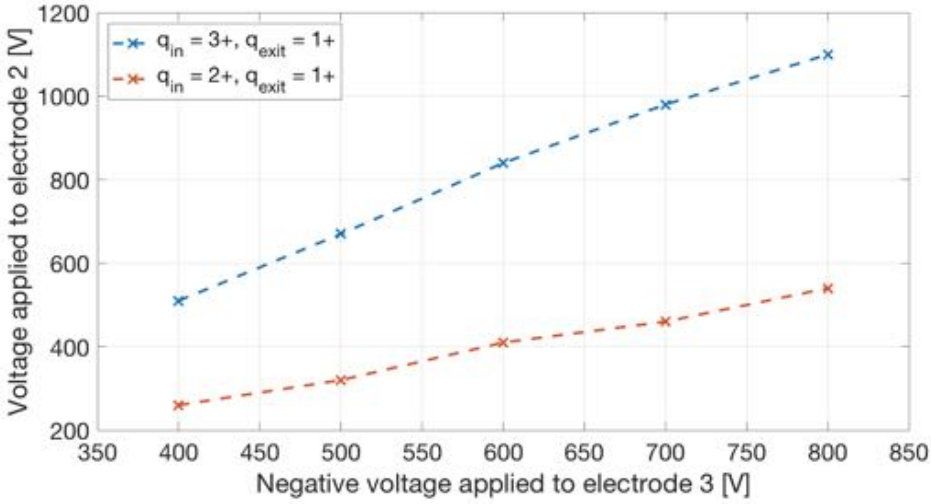

Figure 4.6: Simulation of the variation of the voltage at electrode 3 (CNM) and the voltages that have to be applied to electrode 2 in order to obtain the maximum registered counts.

4.3.2 Measurements

For the following measurements, the setup shown in Fig. 3.2 was used. The variable part of the setup used for charge state separation can be seen in more detail (including the numbering of the electrodes) in Fig. 3.9.

Variation of the voltage applied to the curved plate capacitor (El.2)

In the experiment, $^{229(m)}Th^{3+}$ and $^{229(m)}Th^{2+}$ ions (and a minor part of $^{229(m)}Th^{1+}$ ions) are, in bunches, guided onto the carbon nano membrane (CNM) where they may change their charge state. The three electrodes of the triode are set to the voltages -2 V, -150 V and -300 V and the CNM to a voltage of -800 V throughout the following measurements. -2000 V are applied to the front plate of the MCP. The deflection of the charged particles in the curved capacitor can be varied by varying the voltage at electrode 2 of the curved plate capacitor (see Fig. 3.9).
For a fixed value of voltage applied to electrode 2, a typical measurement is shown in Fig. 4.7.

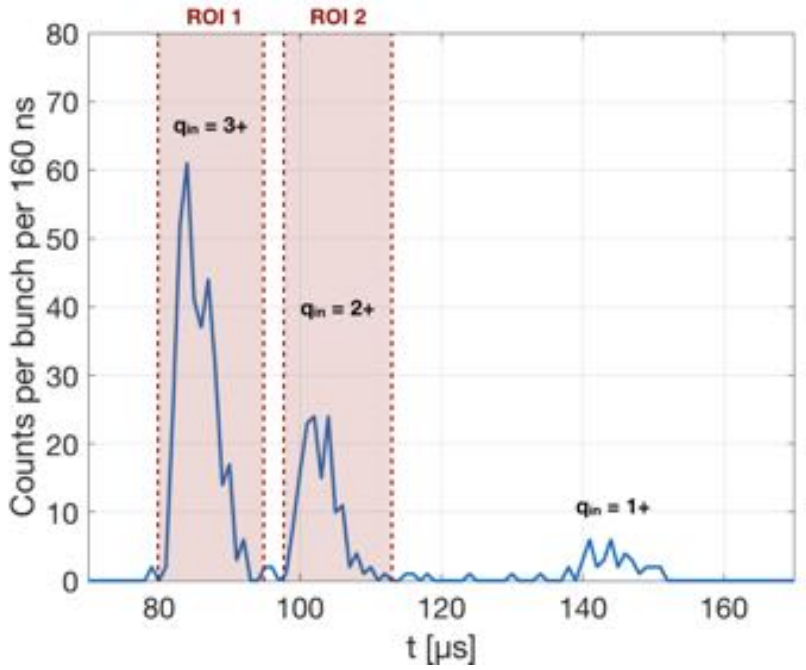

Figure 4.7: A typical measurement result retrieved from the MCP (in this case, for a voltage of 300 V applied to electrode 2). The counts in ROI 1 originate from the incoming $^{229(m)}Th^{3+}$ ions, whereas the counts in ROI 2 originate from the incoming $^{229(m)}Th^{2+}$ ions. Some counts of particles that originate from $^{229(m)}Th^{1+}$ ions are also visible, but will not be of interest in the following analysis. The shown data is based on the detection of 2000 bunches.

The detected signals can be distinguished by their temporal separation. The first peak corresponds to the particles that originate from $^{229m}Th^{3+}$ ions and the second peak to the particles originating from $^{229m}Th^{2+}$ ions. The small peak in the region of about 138 - 150 μs shows the number of registered counts originating from particles that entered the CNM in the 1+ charge state, but will not be considered in the following analysis. The temporal separation is due to the different times of flight in the QMS (see Sect. 3.1). The counts in the two different regions of interest (ROI 1: 80 - 95 μs and ROI 2: 98 -113 μs) are then recorded for varying values of the voltage applied to electrode 2.

For a voltage between 0 V and 15 V applied to electrode 2, the MCP detects a lot of counts in both regions of interest as can be seen in Fig. 4.8.

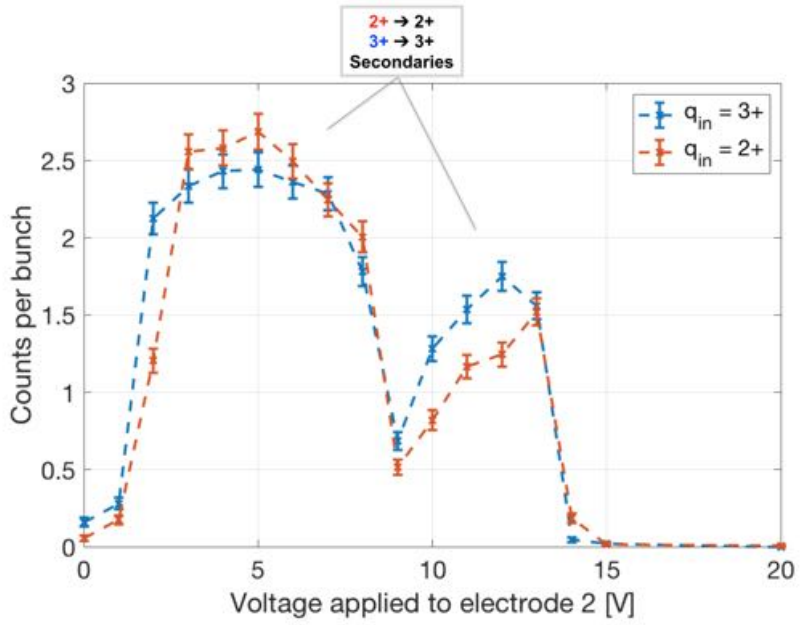

Figure 4.8: Counts recorded for the variation of the voltage applied to electrode 2 in the range of 0 V to 20 V. The shown data is based on the detection of 200 bunches per measurement point.

This could be due to the ions and neutral atoms exiting the CNM and hitting the inner walls of the curved plate capacitor, thereby producing secondary particles (positive low-energy ions) which are then detected. The occurrence of the dip at about 9 V applied to electrode 2 has to be examined in future experiments. This could be done by using a copper grid without a graphene foil in order to not induce charge exchange. This means that for the transmission of the 3+ or 2+ ions (that do not change their charge state) there is no impact of the other charge states or neutralized atoms hitting the inner walls of the curved plate

capacitor. Thus the amount of 3+ or 2+ ions transmitted through the curved plate capacitor without background of secondary particles could be determined.

In Fig. 4.9 the recorded number of counts in the two regions of interest are displayed, which correspond to the incoming 3+ and 2+ charge states for a variation of 20 V to 1600 V at electrode 2.

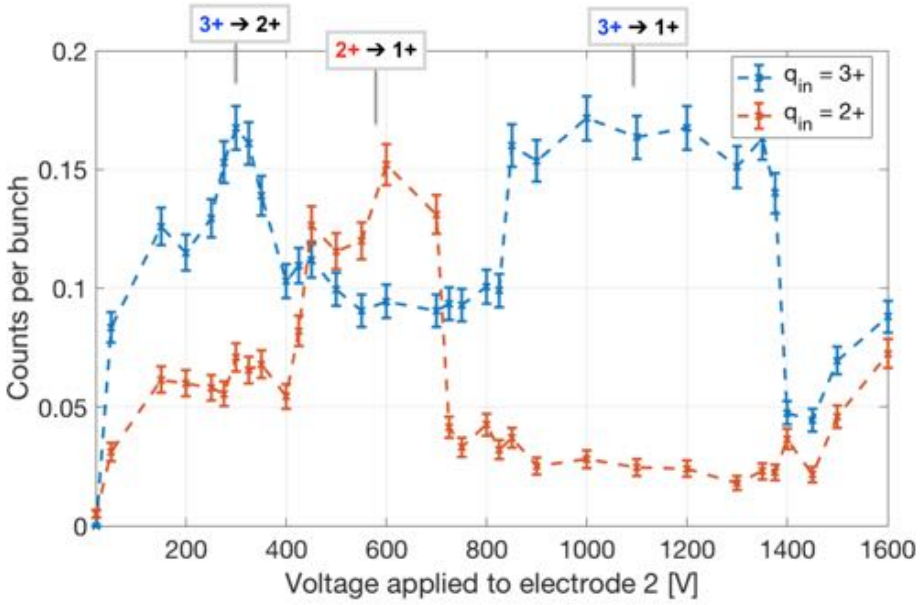

Figure 4.9: Number of counts per bunch recorded as a function of the voltage applied to electrode 2 in the range of 20 V to 1600 V. The shown data is based on the detection of 2000 bunches per measurement point.

On top of a seemingly constant background, which originates from secondary particles, different peaks can be identified. A clear distinction between the peaks is visible. It can be seen that for a voltage of about 430 V to 700 V, the count rate in ROI 2 (2+) is larger than the count rate in ROI 1 (3+), whereas for the other voltages the count rate in ROI 1 dominates (for the definiton of ROI 1, ROI 2 and ROI 3 see Fig. 4.7). Comparing those measurements to the simulations shown in Fig. 4.5, the peaks can be assigned to the different charge-state changes. This leads to the result that a clear distinction of the charge states is not only possible in simulations, but also in the experiment.

For this reason, also the 1+ charge state can be separated from the other charge states. This is one of the prerequisites of enabling a lifetime measurement of $^{229\mathrm{m}}\mathrm{Th}^{1+}$. Regarding the scales of the diagram shown above, it can be seen that only a minor part of the incoming 3+ and 2+ ions changed into singly charged ions. For a quantitative analysis of the efficiency of the generation of $^{229(\mathrm{m})}\mathrm{Th}^{1+}$ see Sect. 4.4.2.

Variation of the voltage applied to the focusing electrode

The influence of the focusing electrode, which is located in front of the CNM, was examined by varying its voltage from -300 V to -800 V in steps of 100 V. During this measurement, the voltage applied to electrode 2 was constantly set to 6 V and the CNM was kept at -800 V. A typical measurement taken for a fixed value of the focusing voltage (in this case, for -600 V) is depicted in Fig. 4.10.

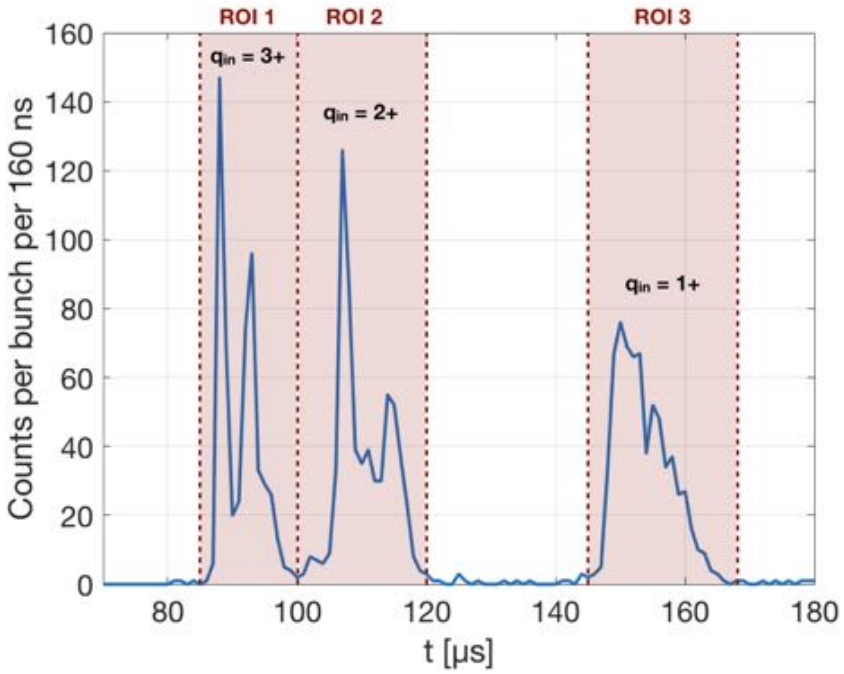

Figure 4.10: Typical measurement result retrieved from the MCP (for a voltage of -600 V applied to the focusing electrode). The shown data is based on the detection of 200 bunches.

The counts detected on the MCP were distinguished in three different ranges of interest ROI 1 (the counts measured between 85 to 100 μs, corresponding to the counts generated by particles originating from the 3+ ions), ROI 2 (100 to 120 μs, corresponding to the counts generated by particles originating from the 2+ ions), ROI 3 (145 to 168 μs, corresponding to the counts generated by particles originating from the 1+ ions).

In Fig. 4.11, it can be seen that the extraction increases for all charge states with a decreasing focusing voltage. Additionally, for a voltage of -800 V applied to the CNM, a voltage lower than -800 V at the focusing electrode is expected to lead to a decreasing number of ions reaching the CNM due to the negative accelerating voltage between the two. The extraction is therefore assumed to be most efficient for a focusing voltage of -800 V (if also -800 V are applied to the CNM).

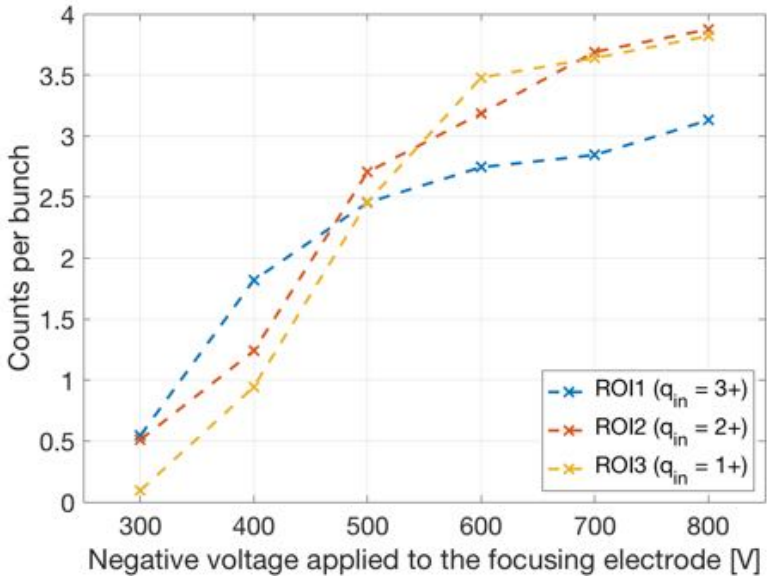

Figure 4.11: Counts in the three regions of interest (as indicated in Fig. 4.10) for varied focusing voltages, while the CNM is kept at -800 V. The shown data is based on the detection of 200 bunches per measurement point. The error bars are smaller than the symbols.

4.4 Quantitative analysis of the resulting extraction efficiencies

The main aim of this thesis is to examine the number of neutral $^{229(\mathrm{m})}$Th atoms that can be generated by sending thorium ions onto a carbon foil and are thus available for the upcoming measurement of the isomeric excitation energy at our group. Furthermore, an efficiency for the $^{229(\mathrm{m})}\mathrm{Th}^{1+}$ ions generated in this process is of interest.

The total efficiencies can be deduced as follows:

$$\epsilon_{\mathrm{tot}}(0+) = \epsilon_{\mathrm{geo}}(0+) \cdot \epsilon_{\mathrm{hole}} \cdot \epsilon_{\mathrm{neutral}} \cdot \epsilon_{\mathrm{det}}(0+), \tag{4.11}$$

$$\epsilon_{\mathrm{tot}}(1+) = \epsilon_{\mathrm{geo}}(1+) \cdot \epsilon_{\mathrm{hole}} \cdot \epsilon_{1+} \cdot \epsilon_{\mathrm{det}}(1+). \tag{4.12}$$

$\epsilon_{\mathrm{geo}}(0+/1+)$ denotes the geometric efficiency, which has to be introduced for those particles being lost on their way due to geometric effects and which is dependent on the examined particle species (0+ $\equiv$ neutral atoms, 1+ $\equiv$ singly charged ions). The value ϵ_{hole} describes the fraction of the incoming ions which pass through holes in the carbon foil and therefore do not experience charge exchange. This value does not depend on the charge state of the particles. The actual neutralization efficiency for ions in the carbon foil is described by $\epsilon_{\mathrm{neutral}}$. Considering the value of the charge equilibrium ($q_{\mathrm{I}} \approx 0.10$) determined in Sect. 2.4, the value of $\epsilon_{\mathrm{neutral}}$ can be assumed to be close to 100 %. The actual efficiency of the generation of singly charged ions in the carbon foil equals to ϵ_{1+}. The efficiency $\epsilon_{\mathrm{det}}(0+/1+)$ equals to the detection efficiency of the MCP detector.

A determination of $\epsilon_{\mathrm{neutral}/1+}$ is of general interest. However, due to the limitations of measurements taken in the course of this thesis, the values of $\epsilon_{\mathrm{geo}}(0+/1+)$ and ϵ_{hole} are unknown. However, a theoretical approximation of $\epsilon_{\mathrm{det}}(0+/1+)$ can be achieved (see Eq. (3.2)).

Therefore, only a combined efficiency of the neutralization as well as for the generation of singly charged ions can be stated as a result, which combines the efficiencies $\epsilon_{\mathrm{geo}}(0+/1+)$, ϵ_{hole} and $\epsilon_{\mathrm{neutral}/1+}$:

$$\epsilon_{\mathrm{comb}}(0+) = \epsilon_{\mathrm{geo}}(0+) \cdot \epsilon_{\mathrm{hole}} \cdot \epsilon_{\mathrm{neutral}}, \tag{4.13}$$

$$\epsilon_{\mathrm{comb}}(1+) = \epsilon_{\mathrm{geo}}(1+) \cdot \epsilon_{\mathrm{hole}} \cdot \epsilon_{1+}. \tag{4.14}$$

In the following, the values for the combined efficiencies are summarized, which can be concluded from the measurements above.

4.4.1 Efficiency for neutralization

An analysis of the efficiency of neutralization is made with the measurements shown in Fig. 4.2.
Considering these measurements, the count rate for neutral atoms seems most efficient for -2000 V applied to the MCP's front plate and -1700 V applied to the graphene foil. For these parameters, the following number of counts per bunch were detected:

$$N_{\text{neutral}}^{\text{measured}} = (51.0 \pm 1)\,\frac{\text{cts}}{\text{bunch}}. \tag{4.15}$$

It is assumed that all of those counts originate from neutral atoms. The kinetic energy of these neutralized ions impinging onto the MCP can be calculated with Eq. (2.13) to be:

$$E_{\text{kin}}(3+ \rightarrow 0+,\, U_{\text{C}} = -1700\,V) = 5.145\,\text{keV}. \tag{4.16}$$

The efficiency of the MCP to detect those particles can, using Eq. (3.2), be approximated to:

$$\epsilon_{\text{det}}(0+) \approx 0.6 \cdot \frac{5.145\,\text{keV}}{\sqrt{229\,\text{u}}} \approx 0.204 \pm 0.02. \tag{4.17}$$

The overall error of the detection efficiency is assumed to be 10 %, to ensure the inclusion of discrepancies with theory.
The approximate number of neutral atoms reaching the MCP detector in this case can then be obtained as follows:

$$N_{\text{neutral}} = \frac{N_{\text{neutral}}^{\text{measured}}}{\epsilon_{\text{det}}(0+)} \approx (250 \pm 25)\,\frac{\text{cts}}{\text{bunch}}. \tag{4.18}$$

Assuming that one bunch of 3+ ions consists of about 400 ions ($N_{\text{in}} = (400 \pm 50)$), the combined efficiency of neutralization can be approximated to:

$$\epsilon_{\text{comb}}(0+) = \frac{N_{\text{neutral}}}{N_{\text{in}}} \approx (62.5 \pm 10)\,\%. \tag{4.19}$$

The uncertainties of N_{neutral} and $\epsilon_{\text{comb}}(0+)$ are obtained via the propagation of uncertainties [28]. The value of the extraction efficiency for neutral atoms is rather high, as predicted. How this result is helpful in the upcoming experiment which aims to determine the isomeric excitation energy of $^{229\text{m}}$Th is explained in Chap. 5.

4.4.2 Efficiency for the extraction of $^{229(\text{m})}\text{Th}^{1+}$ ions

To give an approximate value for the extraction efficiency of $^{229(\text{m})}\text{Th}^{1+}$ ions, the measurements displayed in Fig. 4.9 were analyzed.
The peak assigned to the 1+ ions that were generated by sending 3+ ions through the carbon nano membrane shows approximately $(0.16 \pm 0.01)\ \frac{\text{cts}}{\text{bunch}}$. In the setup used for those measurements, it was assumed that a lot of secondary particles will be able to reach the MCP. The number of secondary particles ($(0.1 \pm 0.01)\ \frac{\text{cts}}{\text{bunch}}$) has to be subtracted from the total number of counts. This leads to the following amount of 1+ ions detected at the MCP in the measurements:

$$N_{1+}^{\text{measured}} \approx (0.06 \pm 0.02)\frac{\text{cts}}{\text{bunch}}. \tag{4.20}$$

The kinetic energy of the 1+ ions is approximated to:

$$E_{\text{kin}}(3+ \rightarrow 1+) \approx 3.6\,\text{keV}. \tag{4.21}$$

The efficiency of the MCP to detect those 1+ ions can be calculated using Eq. (3.2):

$$\epsilon_{\text{det}}(1+) \approx 0.6 \cdot \frac{3.6\,\text{keV}}{\sqrt{229\,\text{u}}} \approx 0.143 \pm 0.015. \tag{4.22}$$

The number of 1+ ions reaching the MCP detector can then be obtained as follows:

$$N_{1+} = \frac{N_{1+}^{\text{measured}}}{\epsilon_{\text{det}}(1+)} \approx (0.42 \pm 0.15)\,\frac{\text{cts}}{\text{bunch}}. \tag{4.23}$$

Assuming that one bunch of 3+ ions consists of about 400 ions ($N_{\text{in}} = (400 \pm 50)$), the combined efficiency of the extraction of $^{229(m)}\text{Th}^{1+}$ ions can be approximated to:

$$\epsilon_{\text{comb}}(1+) = \frac{N_{1+}}{N_{\text{in}}} \approx (0.10 \pm 0.04)\,\%. \tag{4.24}$$

The uncertainties of N_{1+} and $\epsilon_{\mathrm{comb}}(1+)$ are obtained via the propagation of uncertainties [28]. The consequence of this rather low extraction efficiency of singly charged $^{229(\mathrm{m})}$Th ions will be discussed in the next chapter.

5 Conclusion and Outlook

The major motivation of this thesis was to prove that an efficient neutralization of thorium ions can be achieved in a thin carbon foil like graphene. The equilibrium charge predicted in Sect. 2.4 for thorium ions passing through graphene ($q_{\mathrm{I}} \approx 0.10$) is evident in experiments. The major fraction of the ions hitting the carbon foil (excluding those ions that pass through holes in the foil, thus without changing their charge state) were observed to neutralize. Only a minor fraction ended up being singly or doubly charged. A combined efficiency of $(62.5 \pm 10)\,\%$ for the neutralization of thorium ions was deduced from the measurements (see Sect. 4.4.1).

This result is essential for an upcoming measurement of the isomeric excitation energy of the first excited nuclear state of ^{229}Th, which could pave the way for the development of a nuclear clock. In this attempt, the energy of the electron emitted in the internal conversion decay of neutral $^{229\mathrm{m}}$Th is measured using an electron spectrometer (magnetic bottle). As in the setup of our group $^{229(\mathrm{m})}$Th ions are extracted from a buffer-gas stopping cell, neutralization is necessary to allow for a deexcitation of the isomeric state via IC.
In order to reduce background effects caused by ions and electrons in the envisaged IC electron spectroscopy, charged particles have to be suppressed after the neutralization process. The separation of the neutral atoms from the other particles generated at the carbon foil is shown to be possible using blocking electrodes (see Fig. 4.1). This way, collisions of ions with the surfaces of the electron spectrometer can be reduced, which could otherwise lead to an electron emission additional to the internal conversion electrons. The proof of an efficient neutralization in carbon foils and the separation of the generated neutral atoms from other particles is therefore a major step forward towards the success of this experiment.

Furthermore, the possibility of separating the different charge states that exit the carbon foil has been tested using a curved plate capacitor in order to test the efficiency of the $^{229(\mathrm{m})}\mathrm{Th}^{1+}$ extraction. As can be seen in the measurements displayed in Fig. 4.9, a clear differentiation between the exiting charge states can be achieved. However, the analysis of these measurements in Sect. 4.4.2 led to a value of a combined efficiency of the $^{229(\mathrm{m})}\mathrm{Th}^{1+}$ extraction of only about $(0.10 \pm 0.04)\,\%$. The population of the singly charged ions therefore turned out to

be not efficient enough to enable a lifetime measurement of $^{229m}Th^{1+}$, considering that only ~2 % of the extracted singly charged ions will be in the isomeric state $^{229m}Th^{1+}$. This low value of the extraction efficiency also meets the expectations, as the required kinetic energy for the penetrating particles to reach a charge equilibrium of $q_I = 1$ was calculated to about 230 keV (see Sect. 2.4). It has also been proven with other ions like carbon or oxygen that for a higher kinetic energy of the impinging ions the fraction of ions, which end up in the 1+ charge state after penetrating matter, increases [29].

In a future attempt to determine the $^{229m}Th^{1+}$ lifetime, it could therefore be useful to apply a higher voltage to the carbon foil. This would lead to a higher kinetic energy of the ions being pulled onto the carbon foil. It can be estimated that a sufficient population of $^{229(m)}Th^{1+}$ ions in order to make the isomeric decay detectable can only be reached with kinetic energies of the incoming ions larger than 10 keV. Due to the construction of the setup of our group, such high kinetic energies can currently not be achieved without causing high-voltage sparks.

List of Figures

Bibliography

[1] T. H. Nicholson, S. L. Campbell, R. B. Hutson, G. E. Marti, B. J. Bloom, R. L. McNally, W. Zhang, M. D. Barrett, M. S. Safronova, G. F. Strouse, W. L. Tew, and J. Ye. "Systematic evaluation of an atomic clock at 2×10^{-18} total uncertainty". *Nature Communications 6*, 6896, (2015). 1

[2] E. Peik and Chr. Tamm. "Nuclear laser spectroscopy of the 3.5 eV transition in Th-229". *Europhysics Letters 61*, 181–186, (2003). 1

[3] C. J. Campbell, A. G. Radnaev, A. Kuzmich, V. A. Dzuba, V. V. Flambaum, and A. Derevianko. "A Single-Ion Nuclear Clock for Metrology at the 19^{th} Decimal Place". *Physical Review Letters 108*, 120802, (2012). 1

[4] A. D. Ludlow, M. M. Boyd, J. Ye, E. Peik, and P. O. Schmidt. "Optical atomic clocks". *Reviews of Modern Physics 87*, 2, (2015). 1

[5] A. Derevianko and M. Pospelov. "Hunting for topological dark matter with atomic clocks". *Nature Physics 10*, 933–936, (2014). 1

[6] V. V. Flambaum. "Enhanced effect of temporal variation of the fine structure constant and strong interaction in ^{229}Th". *Physical Review Letters 97*, 092502, (2006). 1

[7] C. W. Reich and R. G. Helmer. "Energy Separation of the Doublet of Intrinsic States at the Ground State of ^{229}Th". *Physical Review Letters 64*, 3, (1990). 1.1

[8] R. G. Helmer and C. W. Reich. "An excited state of ^{229}Th at 3.5 eV". *Physical Review C 49*, 1845, (1994).

[9] Z. O. Guimarães-Filho and O. Helene. "Energy of the $3/2^+$ state of ^{229}Th reexamined". *Physical Review C 71*, 044303, (2005).

[10] B. R. Beck, J. A. Becker, P. Beiersdorfer, G. V. Brown, K. J. Moody, C. Y. Wu, J. B. Wilhelmy, F. S. Porter, C. A. Kilbourne, and R. L. Kelley. "Improved Value for the

energy splitting of the ground-state doublet in the ^{229m}Th". *Physical Review Letters 98*, 142501, (2007).

[11] B. R. Beck, C. Y. Wu, P. Beiersdorfer, G. V. Brown, J. A. Becker, K. J. Moody, J. B. Wilhelmy, C. A. Kilbourne, and R. L. Kelley. "Improved Value for the Energy Splitting of the Ground-State Doublet in the Nucleus ^{229m}Th". *LLNL-PROC-415170*, (2009). 1, 2.1

[12] P. V. Borisyuk, E. V. Chubunova, N. N. Kolachevsky, Yu. Yu. Lebedinski, O. S. Vasiliev, and E. V. Tkalya. "Excitation of ^{229}Th nuclei in laser plasma: the energy and half-life of the low-lying isomeric state" . *ArXiv*, 1804.00299, (2018). 1.1

[13] L. von der Wense, B. Seiferle, M. Laatiaoui, J. B. Neumayr, H. Maier, H. Wirth, C. Mokry, J. Runke, K. Eberhardt, C. E. Düllmann, N. G. Trautmann, and P. G. Thirolf. "Direct Detection of the ^{229}Th nuclear clock transition". *Nature 533*, 47–51, (2016). 1, 2.1, 4.1

[14] L. von der Wense. *"On the direct detection of ^{229m}Th"*. PhD thesis, Ludwig-Maximilians-Universität, München, (2016). 2.1, 3.1, 3.3, 3.4, 3.3

[15] B. Seiferle, L. von der Wense, and P. G. Thirolf. "Lifetime measurement of the ^{229}Th Nuclear Isomer". *Physical Review Letters 118*, 042501, (2017). 2.1, 3.1

[16] Wolfgang Demtröder. *"Experimentalphysik 2 - Elektrizität und Optik"*, volume 7. Springer Spektrum, (2017). 2.2

[17] P. Bergveld, J. Hendrikse, and W. Olthuis. "Theory and application of the material work function for chemical sensors based on the field effect principle". *Measurement Science and Technology 9*, 1801–1808, (1998). 2.2

[18] Peter Sigmund. *"Particle Penetration and Radiation Effects - Penetration of Atomic and Molecular Ions"*, volume 2. Springer, (2014). 2.4

[19] N. Bohr and J. Lindhard. "Electron capture and loss by heavy ions penetrating through matter". *Matematisk-fysiske Meddelelser 28*, 2, (1954). 2.4

[20] E. Gruber, R. A. Wilhelm, R. Pya, V. Smejkal, R. Kozubek, A. Hierzenberger, B. C. Bayer, I. Aldazabal, A. K. Kazansky, F. Libisch, A. V. Krasheninnikov, M. Schleberger, S. Facsko, A. G. Borisov, A. Arnau, and F. Aumayr. "Ultrafast electronic response of graphene to a strong and localized electric field". *Nature Communications 7*, 13948, (2016). 2.5, 2.5

[21] L. von der Wense, B. Seiferle, M. Laatiaoui, and P. G. Thirolf. "Determination of the extraction efficiency for ^{233}U source α-recoil ions from the MLL buffer-gas stopping cell". *European Physical Journal A 51*, 29, (2015). 3.1

[22] Micro-to-Nano. "microtonano.com". URL https://www.microtonano.com/EM-Tec-Graphene-TEM-support-films.php. [Accessed on July, 17th 2018]. 3.2

[23] Hamamatsu Photonics K.K. "MCP and MCP assembly". URL https://www.hamamatsu.com/resources/pdf/etd/MCP_TMCP0002E.pdf. [Accessed on August, 5th 2018]. 3.4

[24] J. L. Wiza. "Microchannel plate detectors". *Nuclear Instruments and Methods 162*, 587–601, (1979). 3.4, 3.4

[25] RoentDek Handels GmbH. "List of particle species that can be detected by Micro-Channel Plates and similar secondary electron multipliers". URL https://roentdek.com/products/guidelines/List_of_particle_species.pdf. [Accessed on August, 5th 2018]. 3.4, 4.2

[26] P. Van Duppen, M. Huyse, L. da Costa Pereira, A. Vantomme, M. Verlinde, E. Verstraelen, R. Ferrer, M. Laatiaoui, S. Sels, Yu. Kudryavtsev, S. Cottenier, U. Wahl, J. G. Correia, P. G. Thirolf, L. von der Wense, B. Seiferle, S. Raeder, M. Block, I. Moore, S. Geldhof, M. Reponen, L. Gaffney, V. Fedosseev, B. Marsh, Th. Stora, J. P. Ramos, S. Rothe, E. Peik, U. Köster, and L. M. Fraile. "Characterization of the low-energy ^{229m}Th isomer". *Letter of Intent to the ISOLDE and Neutron Time-of-Flight Committee*, (2017). 4.1

[27] Inc. Scientific Instrument Services. "simion.com". URL https://www.simion.com. [Accessed on July, 17th 2018]. 4.3.1

[28] Wolfgang Demtröder. *"Experimentalphysik 1 - Mechanik und Wärme"*, volume 8. Springer Spektrum, (2018). 4.4.1, 4.4.2

[29] F. Allegrini, R. W. Ebert, S. A. Fuselier, G. Nicolaou, P. Bedworth, S. Sinton, and K. J. Trattner. "Charge state of 1 to 50 keV ions after passing through graphene and ultrathin carbon foils". *Optical Engineering 53(2)*, 024101, (2014). 5

Amersdorffer , Ines
(Nachname, Name)

München, 14.08.2018
(Ort, Datum)

Eidesstattliche Erklärung

Hiermit bestätige ich, dass die vorliegende Arbeit von mir selbständig verfasst wurde und ich keine anderen als die angegebenen Hilfsmittel – insbesondere keine im Quellenverzeichnis nicht benannten Internet-Quellen – benutzt habe und die Arbeit von mir vorher nicht in einem anderen Prüfungsverfahren eingereicht wurde. Die eingereichte schriftliche Fassung entspricht der auf dem elektronischen Speichermedium. Ich bin damit einverstanden, dass die Bachelorarbeit veröffentlicht wird.

_____
(Signature)